

Parametrising Star Formation Histories

Vimal Simha¹, David H. Weinberg², Charlie Conroy³, Romeel Davé^{4,5,6},
Mark Fardal⁷, Neal Katz⁷, Benjamin D. Oppenheimer⁸

¹ *Institute for Computational Cosmology, Department of Physics, Durham University, South Road, Durham DH1 3LE, United Kingdom*
vimal.simha@durham.ac.uk

² *Astronomy Department and Center for Cosmology and AstroParticle Physics, Ohio State University, Columbus, OH 43210, USA*
dhw@astronomy.ohio-state.edu

³ *Department of Astronomy & Astrophysics, University of California, Santa Cruz, CA, USA*

⁴ *University of the Western Cape, Bellville, Cape Town 7535, South Africa*

⁵ *South African Astronomical Observatories, Observatory, Cape Town 7925, South Africa*

⁶ *African Institute for Mathematical Sciences, Muizenberg, Cape Town 7945, South Africa*
rad@astro.as.arizona.edu

⁷ *Astronomy Department, University of Massachusetts at Amherst, MA 01003, fardal,nsk@astro.umass.edu*

⁸ *Center for Astrophysics and Space Astronomy, Department of Astrophysical and Planetary Sciences, University of Colorado, 389 UCB, Boulder, CO 80309, USA; oppenheimer@strw.leidenuniv.nl*

3 April 2014

ABSTRACT

We examine the star formation histories (SFHs) of galaxies in smoothed particle hydrodynamics (SPH) simulations, compare them to parametric models that are commonly used in fitting observed galaxy spectral energy distributions, and examine the efficacy of these parametric models as practical tools for recovering the physical parameters of galaxies. The commonly used τ -model, with $\dot{M}_* \propto e^{-(t-t_i)/\tau}$, provides a poor match to the SFH of our SPH galaxies, with a mismatch between early and late star formation that leads to systematic errors in predicting colours and stellar mass-to-light ratios. A one-parameter lin-exp model, with $\dot{M}_* \propto t e^{-(t-t_i)/\tau}$, is much more successful on average, but it fails to match the late-time behaviour of the bluest, most actively star-forming galaxies and the passive, “red and dead” galaxies. We introduce a 4-parameter model, which transitions from lin-exp to a linear ramp after a transition time t_{tr} , which describes our simulated galaxies very well. In practice, we can fix two parameters (t_i and t_{tr}) without significant loss of accuracy. We test the ability of these parametrised models to recover (at $z = 0, 0.5$, and 1) the stellar mass-to-light ratios, specific star formation rates, and stellar population ages from the galaxy colours, computed from the full SPH star formation histories using the FSPS code of Conroy et al. (2009). Fits with τ -models systematically overestimate M_*/L by ~ 0.2 dex, overestimate population ages by $\sim 1 - 2$ Gyr, and underestimate \dot{M}_*/M_* by ~ 0.05 dex. Fits with lin-exp are less biased on average, but the 4-parameter model yields the best results for the full range of galaxies. Marginalizing over the free parameters of the 4-parameter model leads to slightly larger statistical errors than 1-parameter fits but essentially removes all systematic biases, so this is our recommended procedure for fitting real galaxies.

1 INTRODUCTION

Large samples of galaxies with multi-wavelength photometric data and spectroscopic data (e.g. York et al. 2000; Giavalisco et al. 2004; Scoville et al. 2007) have allowed galaxy evolution studies to shift from luminosity and colour to the more physical plane of stellar mass and star formation rate (SFR), and to examine other aspects of galaxy evolution such as median ages of stellar populations, importance of bursts, correlations with stellar and gas phase metallicity, AGN activity, dust extinction etc. Deep photometric surveys have also renewed emphasis on photometric redshifts, which require a model of intrinsic galaxy colour.

A crucial step in such analyses is fitting a parametric star formation history (SFH) to each galaxy’s observed spectral energy distribution (SED). One of the most commonly used parametrisations is the so called “ τ -model,” where the SFH is described by an exponentially decreasing SFR with e-folding time τ (e.g., Bruzual 1983; Papovich et al. 2001; Shapley et al. 2005; Lee et al. 2009; Pozzetti et al. 2010; Förster Schreiber et al. 2009), sometimes augmented with bursts (e.g., Kauffmann et al. 2003; Brinchmann et al. 2004). Some authors (e.g., Lee et al. 2010) advocate an alternative model where the SFH is parametrised by $t e^{-t/\tau}$, which allows linear growth at early times followed by an ex-

ponential decline at late times. This is sometimes referred to as the “delayed” or “extended” τ -model, but in this paper we shall refer to it as the lin-exp (linear-exponential) model. Another approach is to fit the SFR in bins of time (e.g., Panter et al. 2007; Tojeiro et al. 2009), which has the virtue of generality but places strong demands on the quality of the data and the accuracy of the population synthesis models.

In this paper, we examine which parametrised models give good descriptions for the SFHs of galaxies in smoothed particle hydrodynamics (SPH) simulations. While SPH simulations are not a perfect representation of the real Universe, they provide useful guidance on what functional forms of the SFH may be necessary. The simulations incorporate a wide range of processes that may be important in galaxy SFHs, including accretion with environmental dependence and stochastic variations, minor and major mergers, conversion of gas to stars based on physical conditions in the interstellar medium, ejection of gas in galactic winds, and recycling of this ejected material through subsequent accretion.

Our galaxy SFHs are obtained from a hydrodynamical simulation of a cosmological volume ($50h^{-1}\text{Mpc}$ cube, modeled with 2×288^3 particles) incorporating gas cooling, star formation, and galactic winds driven by star formation. The simulation reproduces the observed stellar mass function and HI mass function of galaxies quite well up to galaxies with stellar mass $M_* \sim 10^{11}M_\odot$ (Oppenheimer et al. 2010; Davé et al. 2013), but it fails at higher masses, predicting galaxies that are more massive than observed and have too much late-time star formation. To obtain a better match to the observed galaxy stellar mass function and colour-magnitude diagram, we also apply a post-processing prescription to the simulation that has the effect of quenching star formation in massive galaxies. Throughout the paper we consider both the galaxy population predicted directly by the simulation and the population that results from applying this post-processing prescription; we refer to the former as the “Winds” population and the latter as the “Winds+Q” population.

We compare parametric models for the SFH of galaxies to the SFH of galaxies in our SPH simulation to investigate how well various parametric forms describe the shape of the SFH of simulated galaxies and how well they predict the colours and mass-to-light ratios of their stellar populations. We then examine the effectiveness of these parametric models as practical tools. We compute the colours of our simulated galaxies using their true SFHs, then fit parametric models to the colours and ask how well these fits recover physical parameters of interest such as the stellar mass, population age, and current star formation rate. Our investigation offers insight into the shortcomings of commonly used SFH models in regard to the biases and errors they introduce in estimates of the physical parameters of galaxies. It also has practical import for future studies of galaxy evolution, as we suggest a new parametric model that describes the full variety of SFHs in our simulations, which can be used straightforwardly to interpret observations of galaxy populations.

Sources of systematic uncertainty in the SED fitting technique have been investigated by several authors. For example, Conroy et al. (2009) investigate uncertainties arising

from the assumed form of the initial mass function (IMF) and the treatment of stellar evolution, Papovich et al. (2001) examine errors introduced by uncertainties in the dust extinction, and Lee et al. (2009) find significant errors and systematic biases when standard methods for inferring ages and stellar masses of Lyman Break Galaxies (LBGs) are applied to mock catalogues constructed from semi-analytic models. Obtaining accurate stellar spectral libraries that cover the full range of stellar populations present in observed galaxies is a particular challenge. (See Conroy 2013 for a review of the stellar population synthesis technique, and inference of physical parameters of galaxies from SEDs.) However, even if these sources of systematic errors are controlled or eliminated, additional systematic uncertainties arise from the assumed shape of the SFH, and to get the most from the data one wants a model that has as much flexibility as needed but not more than is needed. It is this aspect of population synthesis modeling that we focus on in this paper.

In §2, we describe our simulation, our method for identifying halos and galaxies, our prescription for quenching star-formation in massive galaxies, and our parametric SFH models. In §3, we fit these parametric models to the SFHs of our simulated galaxies and ask how well they describe the SFHs and the physical parameters that can be derived from them. In §4, we fit these models to the colours of galaxies and compare the physical parameters obtained from these fits to their “true” values in the simulation. We summarise our results and discuss their implications in §5. The Appendix compares our parametric SFH model to the one proposed recently by Behroozi et al. (2013).

2 METHODS

2.1 Simulation

Our simulation is performed using the GADGET-2 code (Springel 2005) as modified by Oppenheimer & Davé (2008). Gravitational forces are calculated using a combination of the Particle Mesh algorithm (Hockney & Eastwood 1981) for large distances and the hierarchical tree algorithm (Barnes & Hut 1986; Hernquist 1987) for short distances. The SPH algorithm is entropy and energy conserving and is based on Springel & Hernquist (2002). The details of the treatment of radiative cooling can be found in Katz, Weinberg & Hernquist (1996) and Oppenheimer & Davé (2006). The details of the treatment of star formation can be found in Springel & Hernquist (2003). Briefly, each gas particle satisfying a temperature and density criterion is assigned a star formation rate, but the conversion of gaseous material to stellar material proceeds stochastically. The parameters for the star formation model are selected so as to match the $z = 0$ relation between star formation rate and gas density (Kennicutt 1998; Schmidt 1959).

We adopt a Λ CDM cosmology (inflationary cold dark matter with a cosmological constant) with $\Omega_m=0.25$, $\Omega_\Lambda=0.75$, $h \equiv H_0/100 \text{ km s}^{-1}\text{Mpc}^{-1}=0.7$, $\Omega_b = 0.044$, spectral index $n_s = 0.95$, and the amplitude of the mass fluctuations scaled to $\sigma_8 = 0.8$. These values are reasonably close to recent estimates from the cosmic microwave background (Larson et al. 2010) and large scale structure (Reid et al.

2010). We do not expect minor changes in the values of the cosmological parameters to affect our conclusions.

We follow the evolution of 288^3 dark-matter particles and 288^3 gas particles, i.e. just under 50 million particles in total, in a comoving box that is $50h^{-1}$ Mpc on each side, from $z = 129$ to $z = 0$. The dark matter particle mass is $4.3 \times 10^8 M_\odot$, and the SPH particle mass is $9.1 \times 10^7 M_\odot$. The gravitational force softening is a comoving $5h^{-1}$ kpc cubic spline, which is roughly equivalent to a Plummer force softening of $3.5h^{-1}$ kpc. Higher resolution simulations of smaller volumes (e.g., Davé et al. 2013) would yield more accurate SFH predictions at a given stellar mass, but for the purposes of this paper we considered it more important to have good statistics for a wide range of galaxy masses and environments, so we chose to focus on a larger volume simulated at lower resolution. There are also uncertainties associated with the hydrodynamics algorithm itself (e.g., Agertz et al. 2007; Sijacki et al. 2012), but for our purposes these are less important than the physical uncertainties associated with feedback and quenching mechanisms. We discuss how all of these effects might impact our conclusions in §5.

Our simulation incorporates kinetic feedback through momentum driven winds as implemented by Oppenheimer & Davé (2006, 2008), where the details of the implementation can be found. Briefly, wind velocity is proportional to the velocity dispersion of the galactic halo, and the ratio of the gas ejection rate to the star formation rate is inversely proportional to the velocity dispersion of the galactic halo. Except for the differences in volume and particle mass, our simulation is similar to the “vzw” simulations of Oppenheimer et al. (2010), who investigate the growth of galaxies by accretion and wind recycling and compare predicted mass functions to observations. The specific simulation analyzed here was also used by Zu et al. (2010) to investigate intergalactic dust extinction and Simha et al. (2012) to investigate subhalo abundance matching techniques. The vzw model is quite successful at reproducing observations including quasar metal absorption line statistics at high Oppenheimer & Davé (2006) and low (Oppenheimer et al. 2012) redshift, the HI mass function of galaxies at $z = 0$ (Davé et al. 2013), and the galaxy stellar mass function up to luminosities $L \sim L_*$ (Oppenheimer et al. 2010).

We identify dark matter haloes using a FOF (friends-of-friends) algorithm (Davis et al. 1985). The algorithm selects groups of particles in which each particle has at least one neighbour within a linking length, set to the interparticle separation at one-third of the virial overdensity, which is calculated for the value of Ω_M at each redshift using the fitting formula of Kitayama & Suto (1996). Many of our plots distinguish between the behavior of central galaxies of halos and satellite galaxies (see Simha et al. 2009 for discussion). The most massive object in a FOF halo is referred to as a central galaxy and the others as satellites.

Hydrodynamic cosmological simulations that incorporate cooling and star formation produce dense groups of baryons with sizes and masses comparable to the luminous regions of observed galaxies (Katz, Hernquist, & Weinberg 1992; Evrard et al. 1994). We identify galaxies using the

Spline Kernel Interpolative DENMAX (SKID¹) algorithm (Gelb & Bertschinger 1994; Katz, Weinberg & Hernquist 1996), which identifies gravitationally bound particles associated with a common density maximum. We refer to the groups of stars and cold gas thus identified as galaxies. The simulated galaxy population becomes substantially incomplete below a threshold of ~ 64 SPH particles (Murali et al. 2002), which corresponds to a baryonic mass of $5.8 \times 10^9 M_\odot$. For this work, we adopt a higher stellar mass threshold of $10^{10} M_\odot$ because star formation histories of lower mass galaxies are noisy, even if their final stellar masses are reasonably robust.

For each SKID identified galaxy at $z = 0$, we trace the formation time of its stars. We then bin these star formation events in time to extract a star formation rate as a function of time. From this SFR(t), we generate colours using the stellar population synthesis package FSPS (Conroy et al. 2009). We assume solar metallicity and ignore dust extinction in this paper. While dust extinction and metallicity should be additional free parameters when fitting SFHs to colours of observed galaxies, our goal in this paper is to isolate the impact of SFH shape, so we avoid the step of inserting and then attempting to remove these additional effects.

2.2 Quenching Model

The left panel of Figure 1 shows the $(g - r)$ colour of SPH galaxies against their r -band magnitudes. Each point is an individual galaxy. Central galaxies are shown as black crosses and satellite galaxies as green open circles. The red galaxies in our simulation are almost all low luminosity satellites. In common with other hydrodynamic simulations that do not include AGN feedback, our simulation fails to produce bright red galaxies. Our simulation also matches the observed galaxy luminosity function up to L_* but overpredicts the number density of galaxies brighter than L_* . To obtain bright red galaxies and match the observed stellar luminosity function, we construct a “quenched winds” (Winds + Q) population by implementing a post-processing prescription.

Various lines of observational evidence suggest that star formation is quenched in high mass halos. The most commonly invoked explanation is AGN feedback. This could be connected to the transition between cold and hot mode gas accretion (Kereš, Katz, Weinberg, & Davé 2005; Dekel & Birnboim 2006), with AGN feedback being more effective in suppressing the accretion of the hot gas that appears in higher mass halos. In any case, models of galaxy formation that match the observed luminosity function or stellar mass function have some quenching mechanism for central galaxies of high mass halos.

In our simulation we have a complete history of star formation events for each galaxy. We modify the SFR of galaxies based on their parent halo mass at the epoch of each star formation event. In halos more massive than a halo mass threshold, M_{max} , we eliminate all star formation events. In less massive halos we multiply the mass of stars formed by a factor that scales linearly with halo mass down to a halo

¹ <http://www-hpcc.astro.washington.edu/tools/skid.html>

mass M_{\min} , below which we do not alter the star formation rate. The effect of this post-processing can be described as

$$\text{SFR}(\text{winds} + \text{Q}) = \text{SFR}(\text{winds}) \times f(M_H) \quad (1)$$

where M_H is the parent halo mass and

$$f(M_H) = \begin{cases} 1 & \text{if } (M_H < M_{\min}) \\ \Delta M / (M_{\max} - M_{\min}) & \text{if } (M_{\min} < M_H < M_{\max}) \\ 0 & \text{if } (M_H > M_{\max}) \end{cases} \quad (2)$$

and

$$\Delta M = M_{\max} - M_H. \quad (3)$$

We implement this procedure for both central and satellite galaxies.

We set M_{\min} equal to $1.5 \times 10^{12} M_{\odot}$ and M_{\max} equal to $3.5 \times 10^{12} M_{\odot}$. These parameters are chosen to obtain an approximate match to the observed stellar mass function. Oppenheimer et al. (2010) discuss the comparison between the predicted stellar mass functions and observational estimates in some detail. Roughly speaking, our simulation reproduces observational estimates for $M_* < 10^{11} M_{\odot}$, but it predicts excessive galaxy masses (at a given space density) for $M_* > 10^{10.8} M_{\odot}$. Figure 2 shows the galaxy stellar mass function for the simulation (Winds) and for the post-processing prescription implemented here (Winds + Q). While we do not obtain a perfect match, Winds+Q is a substantial improvement over the original simulation results.

The right panel of Figure 1 shows the colour-magnitude diagram for the quenched winds population. While our post-processing does produce a “massive red sequence” of central galaxies, we do not match the detailed properties of the observed colour-magnitude diagram such as its slope. Also, the brightest galaxies in our model are blue, while the brightest observed galaxies are red. (The most massive galaxies in Winds + Q are on the red sequence, but their higher mass-to-light ratios make them less luminous than the most massive blue galaxies.) Gabor et al. (2011) perform a detailed investigation of various post-processing prescriptions, including one similar to our own, and compare them to the observed stellar mass function, slope of the colour-magnitude diagram and other observables. We refer the reader to that paper for a more in depth discussion of physical and observational issues. Clearly our Winds + Q model is not perfect, but it serves our purpose of providing a model population of galaxies that is a reasonable match to observations, including a large population of quenched massive galaxies as in the real universe.

2.3 SFH models

The simplest SFH model we consider is the “ τ -model” where the SFH is described by an exponentially decreasing function with timescale τ , starting at time t_i :

$$\text{SFR}(t - t_i) = A e^{-(t-t_i)/\tau}. \quad (4)$$

Our simulated galaxies show little star formation before 1 Gyr, and we therefore set $t_i = 1$ Gyr; choosing $t_i = 0$ would make the fits to the simulated SFHs systematically worse.

In practice the simulated SFHs rise to a maximum

rather than starting at a high value, so we also consider the lin-exp model with

$$\text{SFR}(t) = A(t - t_i)e^{-(t-t_i)/\tau}. \quad (5)$$

As with the exponential model, we treat τ as a free parameter and set $t_i = 1$ Gyr. In the limit of $\tau \gg t_0$, the lin-exp SFH is simply a linearly rising $\text{SFR}(t)$, while in the limit $\tau \rightarrow 0$ it is a burst at $t = t_i$.

For greater generality we consider a lin-exp model at early times that transitions to a linear ramp at late times:

$$\text{SFR}(t) = \begin{cases} A(t - t_i)e^{-(t-t_i)/\tau} & \text{for } (t \leq t_{\text{trans}}) \\ \text{SFR}(t_{\text{trans}}) + \Gamma(t - t_{\text{trans}}) & \text{for } (t > t_{\text{trans}}). \end{cases} \quad (6)$$

The key feature of this model is that it decouples the late-time SFR (after t_{trans}) from the early-time SFR, though it requires continuity at t_{trans} . The new parameter Γ determines the slope of the SFH at $t > t_{\text{trans}}$, allowing rising, flat, or falling $\text{SFR}(t)$. (In the FSPS code, Γ is referred to as “ $\tan \theta$ ”, where θ is the angle of the linear ramp in the SFR- t plane.) We set $\text{SFR} = 0$ at times when eq. 6 gives a negative result, thus permitting a truly truncated SFH. We can describe the SFHs of our simulated galaxies adequately by setting $t_i = 1$ Gyr and $t_{\text{trans}} = t_0 - 3.5$ Gyr = 10.7 Gyr, so that Γ is the only new free parameter. We refer to this as our “2-parameter model.” Modest changes in Γ values but would not significantly degrade the fits. However, the timing of the SFR transition and the onset of early star formation could be affected by the specific feedback physics and numerical resolution in our simulations, so real galaxies may have greater variety. We therefore also consider a 3-parameter model in which t_{trans} is a fitting parameter and a 4-parameter model in which both t_{trans} and t_i are fitting parameters. The 4-parameter model is the most general one we consider in this paper and the one we advocate for practical applications. Note that lin-exp is a special case of the 4-parameter model with $t_{\text{trans}} = t_0$ and $t_i = 1$ Gyr.

During the course of our investigation, we also explored other possibilities. For example, we considered models like $t^\alpha e^{-t/\tau}$, but rejected them because they added more complexity without significantly improving the performance in describing the SFHs of our simulated galaxies. We also considered other simple extensions of the lin-exp model such as adding a constant late-time component instead of a linear ramp. However, this model proved insufficient to describe the SFH of galaxies in our simulation, which sometimes show a truncation or a rising late-time SFR. Because our simulations rarely show discrete “bursts” of star formation, we did not investigate parametrisations like the τ +burst models of Kauffmann et al. (2003).

3 FITTING MODELS TO SIMULATED SFHS

In this Section, we fit the five parametric models described in §2.3, namely, the τ -model, lin-exp model, and the 2, 3, and 4-parameter models to the SFHs of galaxies in the SPH simulation (the “Winds” population) and the post-processed simulation (the “Winds+Q” population). We choose model

parameters to minimize the cost function

$$C = \int_0^{t_{\max}} \sqrt{(\text{SFR} - \text{SFR}_{\text{model}})^2} dt. \quad (7)$$

We also impose an integral constraint:

$$\int_0^{t_{\max}} \text{SFR}_{\text{model}}(t) dt = \int_0^{t_{\max}} \text{SFR}(t) dt. \quad (8)$$

The mass-to-light ratio, age quantiles of the stellar population, and predicted colours are independent of the normalization of the SFH and are fully determined by the shape alone.

Figure 3 shows the SFH of a representative selection of SPH galaxies. SFR normalized by the stellar mass at $z = 0$ is shown on the vertical axis against time on the horizontal axis. The thick gray solid curve shows the SFH in the simulation, and the other curves show the best-fit models of the different SFH parametrisations. The top row shows blue galaxies, and each successive lower row shows a redder colour. The first three columns from the left show central galaxies in three mass bins, with mass increasing from left to right. The right column shows satellite galaxies, where a satellite galaxy is defined as a SKID group that is not the most massive galaxy in its FOF halo.

An examination of Figure 3 reveals several interesting trends. The SFHs of low mass galaxies show bumps and wiggles, but for the most part the SFHs of individual galaxies are smooth, not punctuated by starbursts and gaps. Other implementations of star formation and feedback physics might lead to burstier behaviour, but if star formation and its associated outflows largely keep pace with accretion as they do in this simulation, then a smooth SFH is the generic outcome. At high z , most simulated galaxies have a gradually increasing SFH, in contrast to the steep increase followed by exponential decline that is mandated by the τ -model. The shape of the peak in the SFH is generally matched by the lin-exp model when we allow a start time of 1 Gyr for star formation to commence. While the slope of $\text{SFR}(t)$ at high redshift varies strongly from galaxy to galaxy, there is little variation around $t_i \approx 1$ Gyr; in particular, we find no examples of galaxies that wait several Gyr before starting to form stars. At low z , the blue galaxies in the top two rows have a rising SFR, while the red galaxies in the lower rows have a falling SFR. The lin-exp model often describes these histories fairly well, but in some cases it cannot, such as the top two panels in the left column and the bottom two panels in the right column.

As shown by Simha et al. (2009), many satellite galaxies in these simulations continue to accrete gas and form stars, in agreement with inferences from observations (Weinmann et al. 2006, 2010; Wetzel et al. 2013). The top two panels in the right column of Figure 3 show two such examples. The third row of the rightmost column shows a satellite galaxy that is not forming stars at $z = 0$. The bottom row of the same column shows a more extreme example, where the SFR is truncated at $t \sim 8$ Gyr, after the galaxy falls into a massive halo. The lin-exp model fails to match these truncated SFHs, predicting a SFR that is too high at $z = 0$ and consequently a colour that is too blue compared to the simulation. For low mass galaxies in the Winds+Q model, we find similar trends to those in Figure 3, but for higher mass galaxies the SFR at late times is systematically

lower, and for the most massive galaxies it is truncated before $z = 0$.

Figure 4 shows the average SFH of galaxies in bins of mass and colour chosen to contain approximately equal numbers of galaxies. As in Figure 3, the first three columns show central galaxies ordered by increasing mass, the fourth column shows satellite galaxies, and the rows are ordered from the bluest quartile to the reddest quartile in each bin. We also show the average stellar mass and the $g - r$ colour obtained by treating the average SFH as the SFH of an individual galaxy and using it as input for the stellar population synthesis code. These curves are smoother than those in Figure 3 because they average over variations in individual SFHs, but they reveal the same trends. The τ -model shows the same systematic failures seen in in Figure 3. The lin-exp model gives a good description of the average SFH in most bins, but it underpredicts the $z = 0$ SFR in the bluest galaxies and overpredicts the $z = 0$ SFR in red satellites. These discrepancies lead to systematic deviations in the predicted colours as shown below.

Figure 5 is similar to Figure 4 but for the Winds + Q model. Results for the lowest mass central galaxies are similar, of course, but for more massive galaxies the SFHs are often truncated at late times and correspondingly more sharply peaked at early times. The lin-exp model is remarkably successful at describing the SFH shape in most of these bins, capturing the correlation between rapid early growth and suppressed late-time star formation. However, it fails to predict the correct $z = 0$ SFR in some cases. We have shown results from the 4-parameter model in Figures 3-5, but the results are only slightly degraded if we fix $t_i = 1$ Gyr (3-parameter model) and $t_{\text{trans}} = 10.7$ Gyr (2-parameter model).

The left panel of Figure 6 compares the $g - r$ colour predicted by the best-fit lin-exp model to the SPH $g - r$ colour. While computing the colours, we ignore dust extinction and use the same SSPs to compute colours from the SFHs for the SPH galaxy and the model fits, and therefore ignore the possibility of template mis-match. Each point is an individual galaxy. Because lin-exp is unable to match the late time increase in SFR for the bluest galaxies, it predicts colours that are systematically too red when $(g - r)_{\text{SPH}} \leq 0.3$. Conversely, for galaxies that are very red, particularly satellite galaxies, it fails to match the truncation in the SFH, instead predicting ongoing star formation and hence colours that are too blue. This error is particularly noticeable for galaxies with $(g - r)_{\text{SPH}} \geq 0.6$. For comparison, the colour from the best-fit 4-parameter model is shown in the right panel. The late time linear component with variable slope helps overcome both these shortcomings of the lin-exp model, yielding accurate colour predictions for the bluest and reddest galaxies. For $(g - r)_{\text{SPH}} = 0.45 - 0.6$ the model colours are still systematically too red. (Recall that all colours in the paper are computed for zero dust reddening.)

Figure 7 shows the distribution of the differences between the colour of the best-fit parametric model and the SPH galaxy whose SFH is fit. We show the 2-parameter and 3-parameter models in addition to the three models shown in Figures 3-5. The τ -model requires too much early star formation relative to late star formation and, therefore, predicts colours that are systematically too red, by ~ 0.15 magnitudes in $u - g$, ~ 0.12 magnitudes in $g - r$, and ~ 0.05

magnitudes in $r - i$. The lin-exp model is mildly biased towards redder colours, but a considerable improvement on the τ -model. Results for the 2, 3, and 4-parameter models are nearly identical and sharply peaked around the colour predicted using the galaxy's true SFH. For the Winds+Q population (right hand panels) the τ and lin-exp models have a low amplitude tail of galaxies whose model colours are much too blue; these are the galaxies with truncated SFHs. This tail is strongly suppressed in the multi-parameter models. As expected, colours at redder wavelengths are predicted more accurately in every case because they are less sensitive to late-time star formation.

One of the most important applications of SED fitting is to infer the mass-to-light ratios of stellar populations, so that observed luminosities can be converted to stellar masses. Figure 8 compares the r -band stellar mass-to-light ratio $Y_r \equiv M_*/L_r$ of SPH galaxies to that obtained from various parametric fits to the SFH. Specifically, we use FSPS to compute r -band luminosities from either the simulated SFH or the SFH of the best-fit parametric model (which is always constrained to reproduce the simulated galaxy's M_*). Because the best-fit τ -model consistently has too much early-time star formation and too little late-time star formation (Figs. 3 and 4), the τ -model fits systematically overestimate Y_r , with a typical offset of 0.2 dex ($Y_{\text{model}}/Y_{\text{SPH}} \sim 1.6$). The lin-exp model fares much better, producing a reasonable match to the mass-to-light ratio of most galaxies but overestimating Y_r for blue galaxies that have an increasing SFR at late times. The 2, 3 and 4-parameter models yield mass-to-light ratios sharply peaked around the true values, fitting 68% of galaxies to within 6%. The right panel shows results for the Winds+Q galaxy population. In addition to the previous trends, the τ and lin-exp models now have a tail of galaxies for which Y_r is underestimated by up to 0.2 dex. These are the red galaxies with sharply truncated SFH, which are poorly represented in these models. The 2, 3, and 4-parameter models, on the other hand, can all represent these truncated SFHs, so they do not produce a tail of underestimated mass-to-light ratios.

We examine the SFHs of galaxies at $z \geq 0$ to investigate whether the parametric models that give good descriptions of $z = 0$ SFHs also do so at $z = 0.5$ and $z = 1$. We fit the five parametric models described in §2.3 to the SFHs of galaxies in the SPH simulation at $z = 1$ and $z = 0.5$. In addition to the lin-exp model described in eq. 5 and the general 4-parameter model described in eq. 6, we also fit a 3-parameter model where we fix $t_i = 1$ Gyr and a 2-parameter model where, in addition, we scale t_{trans} with the age of the Universe. Specifically, we set

$$t_{\text{trans}}(z = z') = t_{\text{trans}}(z = 0) \times t_{z'}/t_0 \quad (9)$$

where t_0 is the age of the Universe at $z = 0$, $t_{\text{trans}}(z = 0) = 10.7$ Gyr is the value previously adopted in our 2-parameter model, and $t_{z'}$ is the age of the Universe at redshift $z = z'$. The 2-parameter model SFH follows a lin-exp model for the first 75% of its lifetime, and a linear ramp thereafter. We restrict our analysis to the Winds + Q model.

Figure 9 shows the distribution of differences between the colour of the best-fit parametric model and the SPH galaxy whose SFH is fit at $z = 1$ (left) and $z = 0.5$ (right) for the Winds + Q model. The lin-exp model is generally biased towards redder colours with the exception of a small number

of galaxies with truncated SFHs whose model colours are too blue. The 4-parameter model is sharply peaked around the colour predicted from the galaxy's true SFH. Fixing $t_i = 1$ Gyr (3-parameter model) produces a nearly identical fit as it is close to the value of t_i obtained from the best-fit 4-parameter model for most galaxies, and in any case small changes in the SFR at early times do not have an appreciable effect on the colour. Further restricting to the 2-parameter model only marginally degrades the fits to the SFH. While the value of t_{trans} fixed according to eq. 9 differs slightly from the mean t_{trans} of the best-fit 4-parameter model to all galaxies, correlations between t_{trans} and Γ ensure that the best-fit 4-parameter SFH and the best-fit 2-parameter SFH are similar even when they have a different t_{trans} . All models predict the redder colours more accurately because they are less sensitive to late-time star formation. As expected, the τ -model (not shown) performs worse at high redshift than at $z = 0$, predicting colours that are too red because it requires too much early star formation relative to late star formation.

Figure 10 compares the r -band mass-to-light ratio, $Y_r \equiv M_*/L_r$ of SPH galaxies to that obtained from various parametric fits to the SFH. The parametric fits are constrained to reproduce the M_* of the SPH galaxy. At both $z = 0.5$ and $z = 1$, the lin-exp model overestimates Y_r for blue galaxies that have an increasing SFR at late times. Additionally, for red galaxies with a truncated SFH, the lin-exp model underestimates Y_r by ~ 0.15 dex. The 2, 3, and 4-parameter models can match both truncated galaxy SFHs and the SFHs of galaxies with a rising SFR at late times, yielding Y_r values sharply peaked around the true Y_r value. They fit 68% of galaxies to within 8% at $z = 1$, and within 13% at $z = 0.5$.

4 FITTING PARAMETRIC MODELS TO GALAXY COLOURS

In dealing with observed galaxies, of course, we do not have a priori knowledge of the SFH. Instead, the SFH and other physical parameters of interest must be inferred from observables like the colours and luminosity. In this Section, we test the efficacy of parametric SFH models as practical tools by fitting them to the colours of galaxies in our simulation and comparing these fits to the true SFHs. We ignore the effects of dust extinction while computing the colours of both SPH galaxies and parametric SFH models. While uncertainties in redshift, dust extinction, and metallicity can introduce additional errors and potential biases, we focus in this work on the effect of the assumed parametrisation of the SFH.

We use the FSPS stellar population synthesis code to compute the luminosity of our simulated galaxies in five SDSS optical bands (u, g, r, i and z), which gives us four colours. We fit our previously described SFH models to these colours assuming a Gaussian error on each colour of 0.02 magnitudes, typical of errors for galaxies in the SDSS spectroscopic sample. While computing the colours, we ignore dust extinction and use the same SSPs to compute colours from the SFHs for the SPH galaxy and the model fits, and therefore ignore the possibility of template mis-match. Our fitting procedure is based on χ^2 minimization. We have implemented our 2, 3, and 4-parameter models as SFH options to FSPS and computed colours on a grid of parameter val-

ues. We interpolate within this pre-computed grid in our χ^2 minimization procedure.

Figure 11 shows the SFH of the same representative sample of SPH galaxies illustrated in Figure 3, and gray bands are repeated from that figure. Now, however, the model curves are found not by minimizing the quantity in equation (7) but by fitting the four colours. As in Figure 3, the solid black curve shows the best-fit 4-parameter model, the dashed red curve shows the best-fit τ -model, and the blue dot-dashed curve shows the best-fit lin-exp model. The top row shows blue galaxies, and each successive lower row shows a redder colour. The first three columns from the left show central galaxies in three mass bins, with mass increasing from left to right, and the extreme right column shows satellite galaxies. For most of our galaxies, the models are formally good fits to the colours given our adopted 0.02 mag errors, though the τ -model sometimes fails to give a statistically acceptable fit for the bluest galaxies.

In nearly all cases, the model fits reproduce the late-time SFH better than the early SFH. This is unsurprising, as the galaxy colour is sensitive to late-time star formation but is minimally affected by moderate shifts of age in the oldest stellar populations. The best-fit τ -model is never a good description of the true galaxy SFH, showing the same generic discrepancies seen in Figures 3-5. The failures are worst for the bluest galaxies, where the τ -model cannot match the rising SFR at late times, and for the reddest galaxies, where the τ -model can produce a truncated SFR at late times only with a strong burst of very early star formation. The lin-exp model provides a good description of the SFH in many cases, for a variety of colours and SFH shapes. The two examples where it fares badly are the satellites with truncated SFHs (right column, two lower panels). Like the τ -model, the single-parameter lin-exp model can only produce very red colours by forcing rapid early star formation, while the actual SFH of these galaxies is more extended before shutting down at late times. The 4-parameter model performs much better than lin-exp for these galaxies, and it reproduces the rising late-time SFR of the bluest galaxies.

For the Winds+Q population we see broadly similar trends, but now the massive central galaxies also have a truncated SFH like the two red satellites in Figure 11. The fraction of galaxies for which the 4-parameter model outperforms lin-exp is, therefore, larger.

In practical applications, fits to observed SEDs are frequently used to infer not the full SFH but high level physical parameters such as stellar mass-to-light ratios (and corresponding stellar masses), population ages, and current star formation rates. Uncertainties in these physical parameters (and, if desired, the covariance of their errors) can be derived by marginalising over the parameters of the fitted model. Figure 12 illustrates this approach for four of the simulated galaxies from Figure 11, showing posterior probability distribution functions (pdfs) of the mass-to-light ratio (left) and median population age (right). For the τ -model and lin-exp model, we adopt a flat prior on τ over the range 0 – 20 Gyr. For the 4-parameter model we adopt the same prior on τ , a flat prior on t_i over the range 0 – 1 Gyr, a flat prior on t_{trans} over the range 6 – 14.16 Gyr (t_0 in our simulation), and a flat prior on $\theta = \tan^{-1} \Gamma$ such that the angle of the linear ramp can range uniformly from $\theta = -\pi/2$ (instantaneous truncation) to $\theta = \pi/3$ (steeply rising).

The top two rows show the mass-to-light ratio and t_{50} of galaxies shown in rows 3 and 4, respectively, of column 3 of Figure 11. For both these galaxies, all three models fit to the galaxy colours reproduce the SFH reasonably well. The most probable Y and t_{50} for the τ -model and the lin-exp model are reasonably close to the true SPH values, although the true value is sometimes outside the formal 95% confidence interval. Because of its greater flexibility, the 4-parameter model allows a larger range of Y and t_{50} , but the peak of the posterior pdfs are very close to the true values, and the true values are always within the 68% confidence interval. The bottom two panels show galaxies whose SFH is truncated (rows 3 and 4 of column 4 in Figure 11). As discussed earlier, both the τ -model and the lin-exp model fail to match the truncated SFH, instead putting too much star formation at early times to match the SPH colours. Because they overpredict the age of the stellar population, they overpredict the mass-to-light ratio. In contrast, the 4-parameter model, which matches the truncation in the SFH, predicts a posterior probability distribution for the mass-to-light ratio whose peak is remarkably close to the true value for both galaxies. The true value of t_{50} is within the 4-parameter model predicted 95% confidence interval in one case (third row), and is very close to the peak of the posterior probability distribution in the other (bottom row).

When investigating statistics for a large population of galaxies (e.g., the galaxy stellar mass function), it is common practice to take the best-fit model parameters for each individual galaxy, though a more sophisticated analysis could consider the full posterior pdf on a galaxy-by-galaxy basis. In what follows we will take the “best-fit” value of a parameter to mean the mode of that parameter’s posterior PDF. Each panel of Figure 13 plots the best-fit stellar mass-to-light ratio from a lin-exp (left) or 4-parameter (right) model fit to the colours of individual SPH galaxies against the galaxies’ true mass-to-light ratios. The mass-to-light ratios in the SPH Winds population (top row) range from $\sim 0.4Y_{\odot}$ to $\sim 3Y_{\odot}$, where $Y_{\odot} = 1M_{\odot}/L_{\odot}$. For the bluer galaxies, with $Y < 2Y_{\odot}$, the lin-exp model predicts Y quite accurately, though SPH galaxies with steeply rising late-time SFR have mass-to-light ratios lower than the minimum value $Y \approx 0.8Y_{\odot}$ that the lin-exp model can produce (with τ forced to its limiting value of 20 Gyr). The behaviour for the red galaxies with a truncated SFR is more problematic. Because lin-exp does not allow sharp truncation, it attempts to produce red colours by forcing star formation very early (see the lower right panels of Fig. 11). As a result, the lin-exp fits overpredict the true Y for these galaxies. The 4-parameter model yields a good correlation between the best-fit Y and the true value across the full range, with only a small number of outliers. The performance for the Winds+Q population (lower panels) is similar in both cases, but now the fraction of “red and dead” galaxies at large Y is higher because it includes massive centrals.

Figure 14 shows the distribution of the differences between the mass-to-light ratios obtained from fitting different parametric models to the optical colours of galaxies and their mass-to-light ratios in the simulation. The τ -model typically overestimates the mass-to-light ratio by a factor of ~ 1.5 , but the error can be as high as a factor of ~ 3 . The lin-exp model generally does better, but it makes significant errors in either direction. Most notably, as already seen in Figure 13,

it overpredicts Y for the reddest galaxies, producing the tail at high $Y_{\text{model}}/Y_{\text{SPH}}$ in Figure 14. The 4-parameter model estimate for the mass-to-light ratio is within 10% of the true value for 68% of galaxies in the Winds and Winds+Q populations, though it shows a weaker version of the same asymmetry seen for lin-exp.

Figure 15 presents a similar analysis for stellar population ages, showing the distribution of differences between model fit values and SPH galaxy values for the times when 10% (t_{10} , top row), 50% (t_{50} , middle row), and 90% (t_{90} , bottom row) of the stars have formed. The 4-parameter model correctly predicts t_{10} and t_{50} to within 1 Gyr and t_{90} to within 0.3 Gyr for 68% of galaxies in both the Winds and Winds+Q populations, and it shows no significant bias, though the tails of the difference distribution are slightly asymmetric. The distribution for lin-exp is qualitatively similar, but it is biased towards high t_{10} and t_{50} by 0.5–1 Gyr, and the distribution for t_{90} is less sharply peaked. The τ -model fits are systematically biased towards older population ages (smaller t_{10} , t_{50} , and t_{90}), by 1–2 Gyr for t_{10} and t_{50} and by 1 Gyr for t_{90} .

Figure 16 shows similar results for specific star formation rates (sSFR $\equiv \dot{M}_*/M_*$) at $z = 0$. For context, inset panels show the histograms of sSFR in the two galaxy populations. Since sSFR is strongly correlated with colour at $z = 0$, models fit to the colours generally reproduce the sSFR quite accurately. However, the τ -model is unable to match the colours of galaxies with rising late-time SFR, and it consequently underestimates their sSFR. All models successfully reproduce low sSFRs for the reddest galaxies, so the peak at near-perfect agreement is higher in the Winds+Q population, where the proportion of such galaxies is larger. *Fractional* errors in the sSFR can be large when the value is extremely small, but for most purposes it is the absolute error that is more relevant. We have carried out the same analyses shown in Figures 14–16 at $z = 0.5$ and $z = 1$, for the same rest-frame colours. While we do not show the plots here, the trends are similar, with the 4-parameter model producing moderate improvements over lin-exp and substantial improvements over the τ -model in recovering stellar mass-to-light ratios, population ages, and sSFRs. We have also checked that using the 2-parameter model with our recommended choices of t_i and $t_{\text{trans}}(z)$ yields similar results to those of the 4-parameter model.

The τ -model, which enforces declining SFHs, fails to match the mass-to-light ratios and stellar population ages of blue galaxies with ongoing star formation, often over predicting the ratios by a factor of ~ 2 . The lin-exp model performs better, providing more precise estimates, but it is often biased. In contrast, the 4-parameter model matches the physical parameters of SPH galaxies quite well. In the 4-parameter model, the individual parameters have partially degenerate effects on the SFH, but this degeneracy does not degrade the determinations of these physical quantities, since a similar SFH implies similar quantities and a similar fit to the data regardless of what parameter combinations produce it. With limited data (e.g., two or three colours, or large colour errors), individual model parameters may be poorly determined, but physical quantities may still be well constrained after marginalization.

So far, we have only considered optical colours. We have also examined the effects of adding IR and UV colours to

the optical data. Specifically, we compute SPH galaxy fluxes in the 2MASS J, H, and K bands and the GALEX NUV and FUV bands, and fit models to the combined data sets again assuming an error of 0.02 magnitudes on each colour. Figure 17 shows the distribution of errors in Y and sSFR from fits of the 4-parameter model to optical colours alone, optical+IR colours, and optical+IR+UV colours. Somewhat surprisingly, adding IR and UV colours does not noticeably reduce the scatter in recovering Y or sSFR; at least with regard to our 4-parameter model, the optical colours already contain all of the relevant information. We find similar results for population ages. Note, however, that we have not included dust extinction or metallicity in our models, and we have assumed that galaxy redshifts are known so that the rest-frame colours are available. Since optical colours already suffice to constrain the SFH in our framework, the additional information in IR and UV data can be applied to constrain extinction, metallicity, and (if necessary) redshift. Broad wavelength coverage is especially important in photometric redshift studies, as UV and IR data help to unambiguously identify breaks in the SED.

5 DISCUSSION

The star formation histories (SFHs) of galaxies in our SPH simulations are generally smooth, governed by the interplay between cosmological accretion and star-formation driven outflow. As a result, they can be well described by models with a small number of free parameters, and this remains true after we implement a post-processing quenching scheme designed to reproduce the observed red colours and stellar mass distributions of the central galaxies in massive halos. While the simulations are far from perfect, they include many realistic aspects of cosmological growth, gas dynamics and cooling physics, and feedback. They can, therefore, provide guidance to the classes of models that are most useful for fitting observed galaxy populations.

One of the models most commonly used for this purpose, the exponentially decaying “ τ -model”, gives a quite poor representation of our simulated galaxies because of its implicit assumption that star formation is most rapid at the earliest epochs and declines thereafter. Adding an initial burst to a τ -model would only exacerbate this problem, and allowing a start at $t_i > 0$ helps but only moderately. Fitting the colours of our simulated galaxies with a τ -model (with start time $t_i = 1$ Gyr) leads to inferred stellar mass-to-light ratios that are systematically too high, by a typical factor ~ 1.5 , and to inferred stellar population ages that are too large, typically by 1–2 Gyr. Inferred specific star formation rates (sSFRs) can be either too high or too low, with substantial scatter about the true values.

The lin-exp model, with $\dot{M}_* \propto (t - t_i) \exp[-(t - t_i)/\tau]$, gives a much better description of the time profiles of star formation in our simulation. We find little star formation in our simulations before $t = 1$ Gyr, reflecting the time required to build up massive systems that can support vigorous star formation, so the model is improved by setting $t_i = 1$ Gyr instead of $t_i = 0$. Fitting the lin-exp model to the optical colors of SPH galaxies largely removes the biases in M/L ratios and population ages that arise with τ -model fitting, and it reduces the scatter between the inferred and true

values for these quantities and for sSFRs. If one is going to fit a galaxy SFH with a one-parameter model, the lin-exp model with $t_i = 1$ Gyr is the one to choose.

The shortcoming of the lin-exp model is that it ties late-time star formation to early star-formation: a rapid early build-up (short τ) necessarily implies a low sSFR at low redshift. Early and late star formation are correlated in SPH galaxies, but they are not so perfectly correlated that galaxies lie on a 1-parameter family of SFH. Our 2-parameter model avoids this problem by changing from lin-exp to a linear ramp after $t_{\text{trans}} = 10.7$ Gyr, decoupling early and late evolution. For many galaxies, this additional freedom makes little difference, but the two-parameter model offers a significantly better description of the bluest galaxies, which have rising star formation rates at late times, and of the reddest galaxies, which have truncated star formation. Fitting galaxy colors with the 2-parameter model removes the small systematic biases in M/L , population ages, and sSFRs that remain with lin-exp fitting, and it reduces the scatter between the true and fitted values.

Our 3-parameter model turns t_{trans} into a fit parameter instead of fixing it at 10.7 Gyr (or more generally 75% of the current cosmic time), and our 4-parameter model additionally turns the start time t_i into a fit parameter. This additional freedom only marginally improves the description of SPH galaxy SFHs or the accuracy of inferred parameter values. However, it avoids hard-wiring these ages into the model, and it provides some safeguard against the possibility that they are too strongly tied to the specifics of our simulation. For example, the preference for $t_i \approx 1$ Gyr could be affected by our mass resolution. In spot checks on a simulation with the same volume but $8\times$ higher mass resolution, which became available after we had completed most of our analysis, we find that all of our results for galaxy SFHs continue to hold, but the best fit value for t_i shifts slightly, from 1 Gyr to 0.83 Gyr.

Our recommended strategy, therefore, is to adopt the 4-parameter model for fitting galaxy colours or SEDs and marginalize over model parameters when computing physical quantities of interest such as M/L ratios, population ages, and specific star-formation rates. To enable this approach, we have added the 4-parameter model as an option to the FSPS population synthesis code (Conroy et al. 2009).² In addition to colours, the FSPS code can compute full galaxy spectra for fitting to spectroscopic data. In place of marginalization, a less laborious but less robust strategy is to estimate physical quantities from the best-fit 2-parameter model, with t_i and t_{trans} fixed to our recommended fiducial values. For our SPH galaxies, this procedure actually yields a *better* match between inferred and true quantities because the adopted priors on t_i and t_{trans} are a good match to the simulations. However, these priors may be overly strong for fitting real galaxies, and the marginalization approach with the 4-parameter model is more conservative.

When fitting the *ugriz* colours of our SPH galaxies at $z = 0$, assuming 0.02 mag colour errors, we are able to determine r -band mass-to-light ratios with typical errors of $\pm 13\%$ (the range encompassing 68% of simulated galaxies). The corresponding error for median population age is

0.9 Gyr, and t_{90} , the time by which 90% of stars form, has a smaller error of 0.3 Gyr. Adding near-UV or near-IR colors produces little further improvement because these quantities are already well determined given the assumed *ugriz* errors, and additional wavelengths do little to break the degeneracies in the 4-parameter model. When fitting real galaxies, one would also need to include dust extinction as an additional parameter with an assumed extinction law (or marginalizing over a range of extinction laws). Including dust extinction will only moderately increase M/L uncertainties because reddening induced by dust or by increased stellar population age has a similar impact on M/L (Bell & de Jong 2001). Conversely, dust extinction increases sSFR uncertainty because increasing dust or increasing late-time star formation have opposite effects on galaxy colours. In the absence of spectroscopic redshifts, one also needs to fit for galaxy photo- z along with the stellar population quantities. In this situation, UV or near-IR data may play a more critical role, breaking degeneracies among SFH, extinction, and redshift. However, we caution that Taylor et al. (2011) find that SPS models do not provide good fits to the full optical-to-NIR SEDs of the galaxies they observe, possibly indicating inconsistencies between the SED shapes of real galaxies and those of the models.

We have extended our analysis to higher redshifts, finding that at $z = 0.5$ and $z = 1$ the lin-exp model suffers from similar shortcomings as at $z = 0$, which are overcome by models that decouple the early and late SFRs. Our 2-parameter model, with $t_i = 1$ Gyr and t_{trans} scaled by the age of Universe, provides a significantly better description of the SFH of SPH galaxies. As at $z = 0$, allowing t_i and t_{trans} to be free parameters only marginally improves the description of SPH galaxy SFHs. At all redshifts, one should bear in mind that our simulation models galaxies with $M_* > 10^{10} M_\odot$, and that the SFHs that characterize much lower mass galaxies could be different both in overall form and in the level of stochasticity.

Sources of uncertainty in the SED fitting technique at even higher redshifts have been investigated by other authors. Lee et al. (2010) apply standard SED fitting techniques to infer the physical parameters of Lyman Break Galaxies at $z \sim 3.4-5$ in a mock catalogue constructed from semi-analytic models of galaxy formation, finding that SFRs are systematically underestimated and mean stellar population ages overestimated because of differences between the galaxy SFHs predicted by their semi-analytic models and the τ -model SFH assumed in their SED fitting technique. Because of the mass resolution of our simulation, the SFHs of $z \geq 2$ galaxies are too noisy to allow us to carry out a direct comparison, but our results at $z \leq 1$ are qualitatively similar to their high z results, highlighting similar discrepancies in the commonly used τ -model SFH.

Fitting the low-order parametrised models presented here should be more precise than fitting general stepwise SFHs. In essence, one is imposing a prior of approximate continuity to extract more from the data and reject pathological fits. This approach may also be more robust to uncertainties in the population synthesis models, since the strong spectral features that appear in stellar populations at specific ages may lead to artificial features in stepwise SFH fits. However, it is possible that the SFHs of real galaxies are more complex than those of our simulated galaxies, with

² Publicly available at <http://code.google.com/p/fsp/>.

bursts playing a more important role or truncation followed by rejuvenation. It will be interesting to search for evidence of such deviations to better constrain the potential contribution of “punctuated” star formation in galaxies of different stellar mass or morphology, or even in individual components of galaxies. These searches can be best carried out with full spectroscopic data rather than with colors alone, or better yet, with resolved stellar populations in nearby galaxies.

ACKNOWLEDGEMENTS

We acknowledge support from NASA ATP grant NNX10AJ95G.

APPENDIX: COMPARISON WITH BEHROOZI SFH PARAMETRISATION

Behroozi et al. (2013) advocate a parametrisation of the SFH based on reconstruction of average SFHs using observed galaxy stellar mass functions, specific star formation rates and cosmic star formation rates. The functional form they advocate is given by:

$$\text{SFR}(t) = A [(t/\tau)^B + (t/\tau)^{-C}]^{-1}. \quad (10)$$

This model contains three free parameters, τ , B and C , in addition to the overall normalization A . We fit this model to the SFHs of SPH galaxies allowing B and C to vary between 0 and 25.

Figure 18 shows the result of fitting this model to the average SFH of galaxies in the Winds + Q model in bins of mass and colour. We show the same set of SFHs as Figure 5. For most galaxies, this model provides a good description of the early SFH. However, because it ties the late time SFR to the early SFR, it does not adequately match the SFH of galaxies with a rising SFR at late times such as those in the top two rows of the left most column. SFHs that are flat or gradually declining at late times are generally well described by the B-model, although for a significant fraction of galaxies, the B-model fails to match the late time SFH. But unlike the lin-exp model, the Behroozi et al. (2013) parametrisation can match truncated SFHs well by employing a large value of B , and a value of C close to 0. The B-model generally provides a substantially better description of the SFH of SPH galaxies than the τ -model or the lin-exp model, but it does not perform as well as the 4-parameter model.

In practice, our 2-parameter model fits the SFH of SPH galaxies nearly as well as our 4-parameter model, and significantly better than equation 10 in situations where they disagree. Thus, the better performance of our model owes to its functional form that decouples early and late-time star formation, and not to the number of parameters.

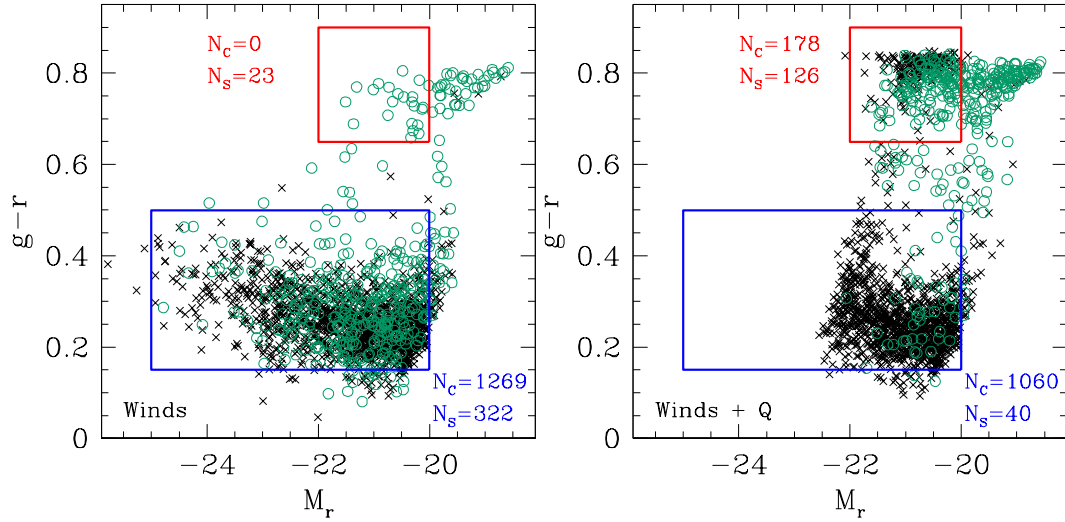


Figure 1. The colour-magnitude diagram of galaxies in our SPH simulation (Winds; left) and after applying our post-processing, quenching prescription (Winds +Q; right). Each point is an individual galaxy. Green open circles are satellite galaxies and black crosses are central galaxies. Since saturation makes it difficult to judge the relative numbers of central and satellite galaxies, we list these numbers for the two boxed regions in each panel. Note in particular that the red sequence is almost entirely populated by satellite galaxies in the Winds model but is dominated (at the bright end) by central galaxies in the Winds+Q model. N_C and N_S denote the number of central and satellite galaxies in each box, respectively.

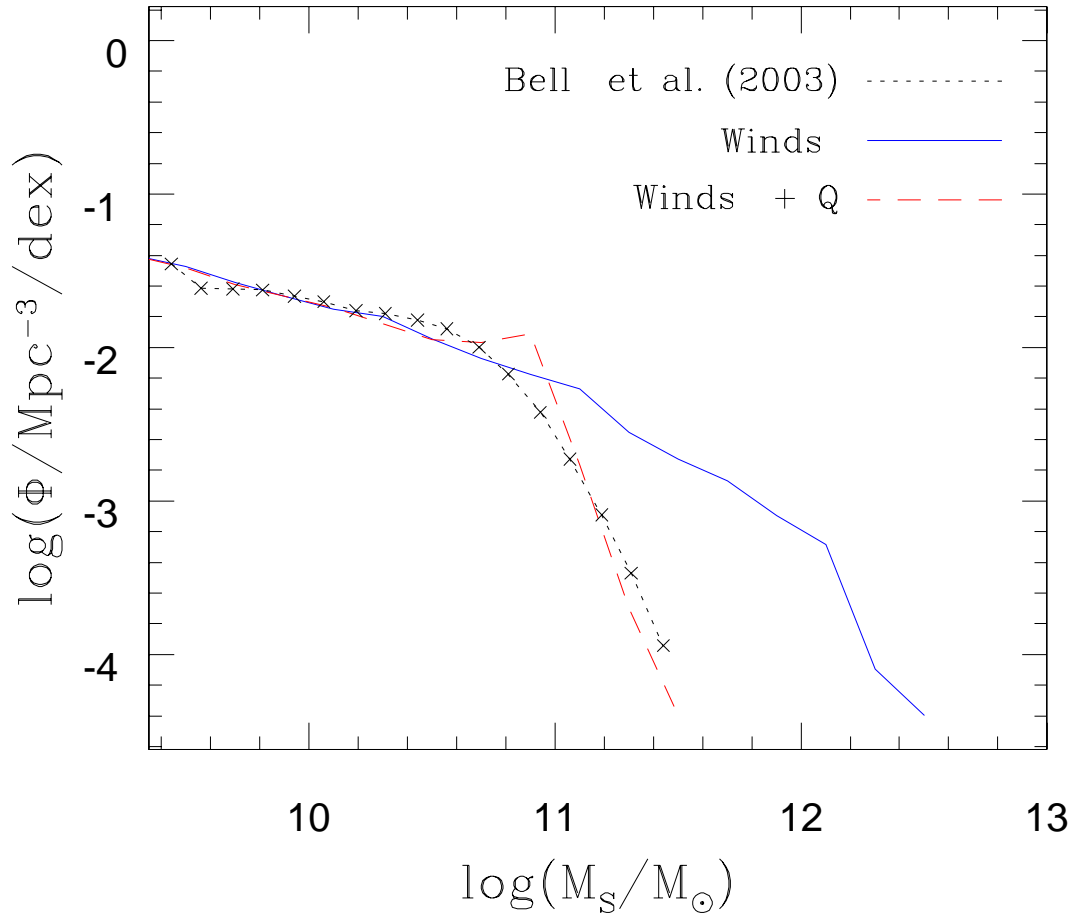


Figure 2. The galaxy stellar mass function at $z = 0$ in our simulation (solid), and after applying our quenched winds post-processing prescription (dashed) compared to the observations of Bell et al. 2003 (dotted). In this and later plots, M_S refers to the stellar mass of SKID-identified galaxies.

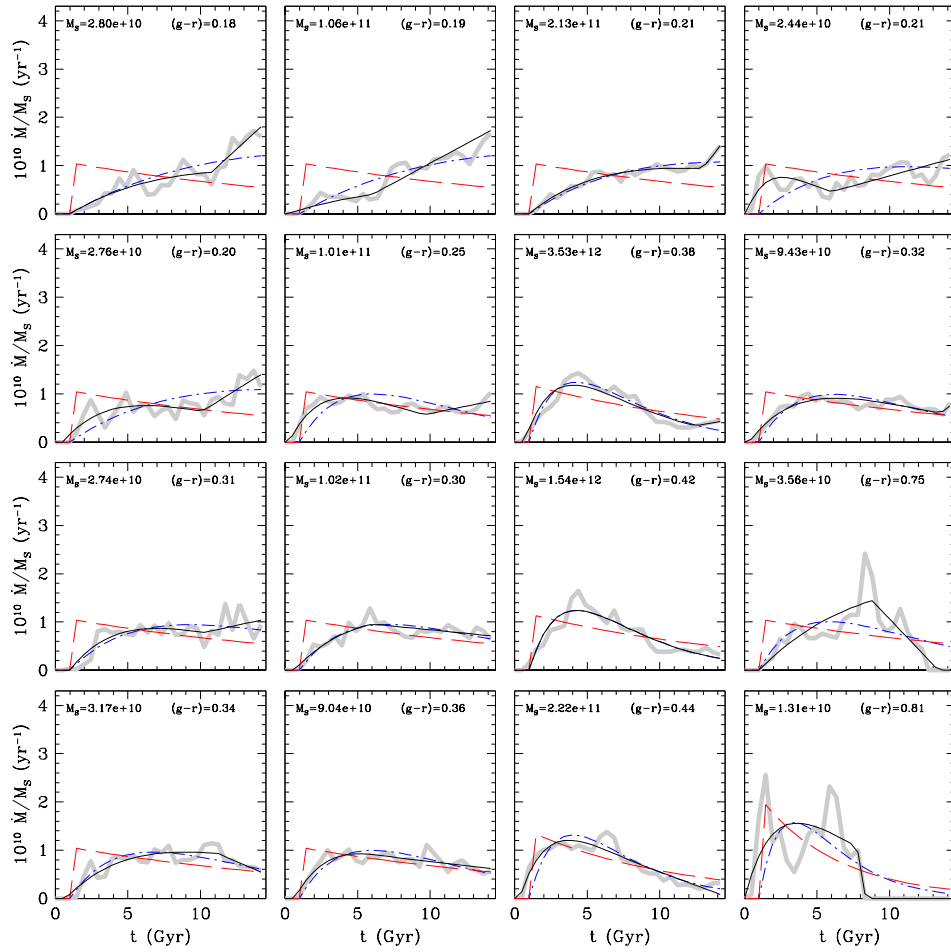


Figure 3. Galaxy SFR versus time in the winds simulation. Each panel shows an individual galaxy. The thick gray curve shows the SFR in the simulation, the black solid curve shows the best-fit 4-parameter model (see text), the blue curve shows the best-fit lin-exp model, and the red curve shows the τ -model. The first three columns from the left show central galaxies in three mass bins, with mass increasing from left to right, and the right column shows satellite galaxies. The top row shows blue galaxies and each successive lower row shows a redder colour.

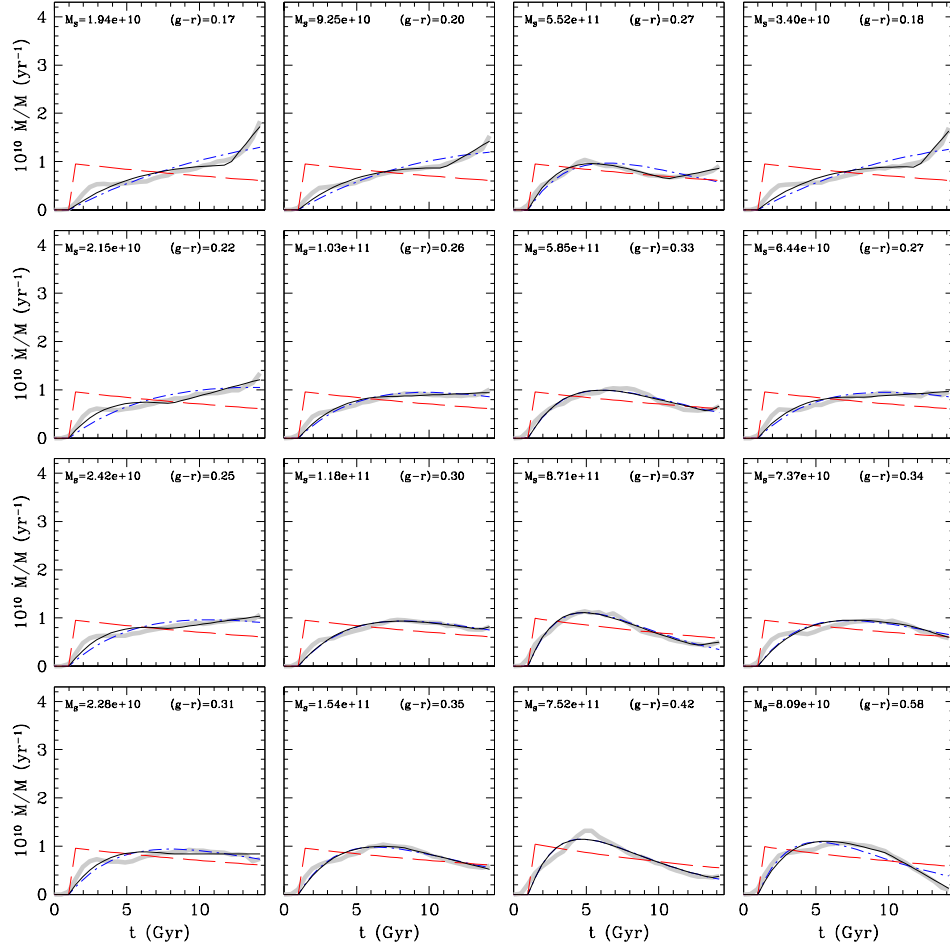


Figure 4. Like Figure 3, but now showing the average SFH of central galaxies in bins of mass and colour (left three columns) and of satellite galaxies in bins of colour (right column). The three central galaxy mass bins are chosen to contain approximately equal numbers of galaxies, and in each column the four panels show the four quartiles of the colour distribution in that bin. Labels indicate the mean stellar mass in each bin and the colour computed by FSPS from the average SFH. Note that the dot-dashed curve (lin-exp) is sometimes fully obscured by the solid curve (4-parameter model), and that the 4-parameter model fit is itself often obscured by the true average SFH.

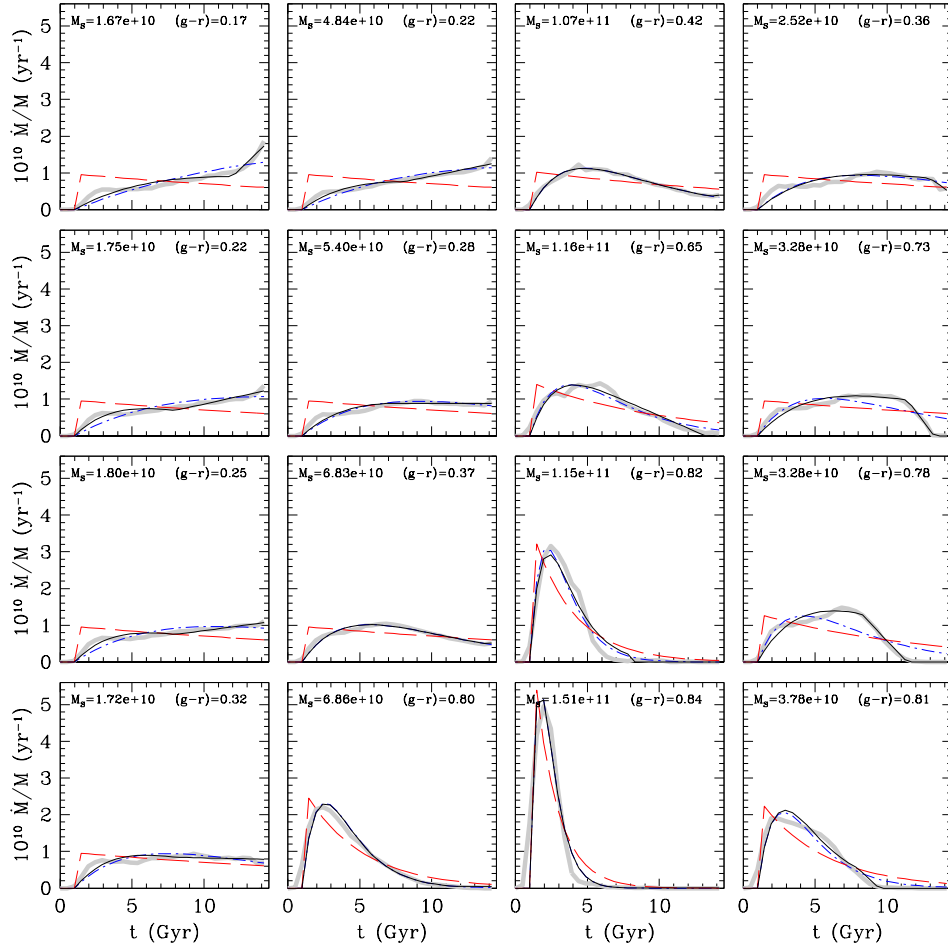


Figure 5. Same as Figure 4, but for the Winds + Q population.

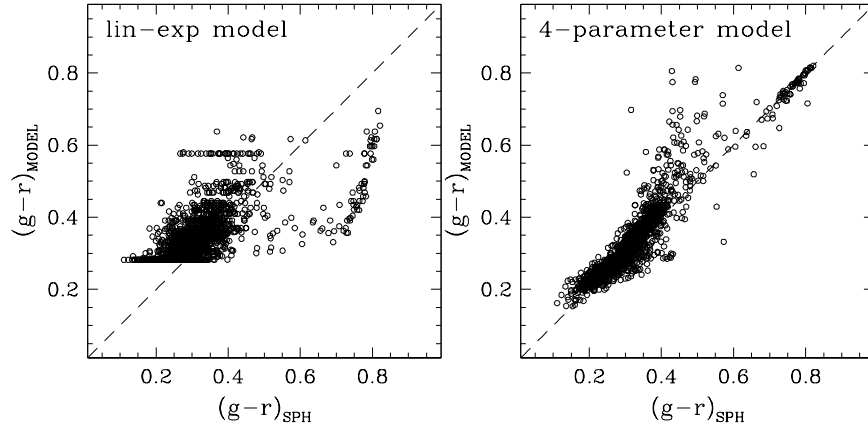


Figure 6. (Left) Colour predicted by the best-fit lin-exp model versus the colour computed from the full SFH of the corresponding SPH galaxy, at $z = 0$. (Right) Same, for the best-fit 4-parameter model. Both panels are for the Winds galaxy population. There are 1,828 individual galaxies in the plot. The horizontal ridges in the left panel correspond to fits with very long or very short timescale τ .

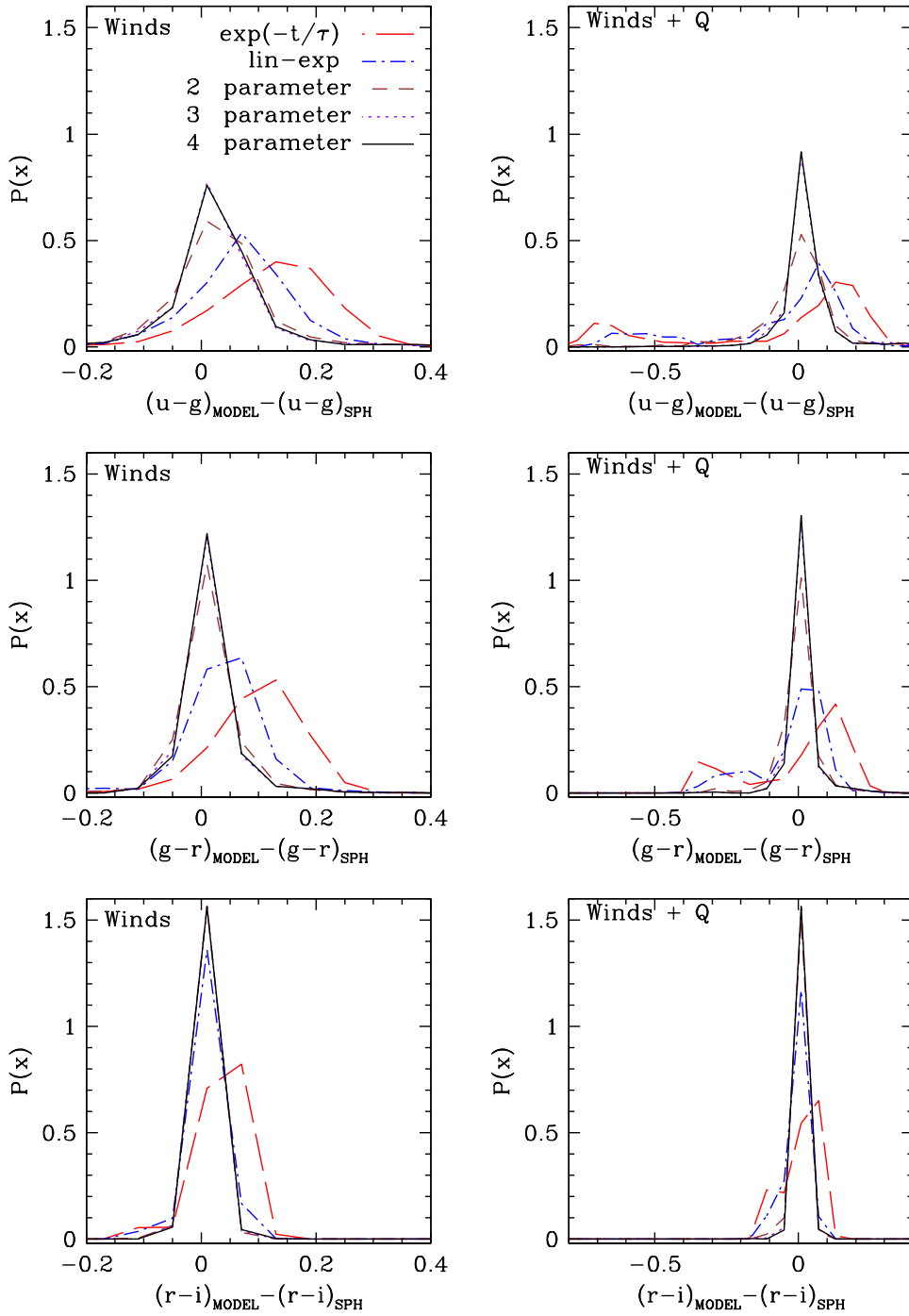


Figure 7. Distribution of differences between parametric model colour and SPH galaxy colour in the winds simulation (left) and the Winds + Q model (right), at $z = 0$. Each curve stands for a different parametric model, and the curves are normalised to unit integral. We ignore the effects of dust extinction on the colours.

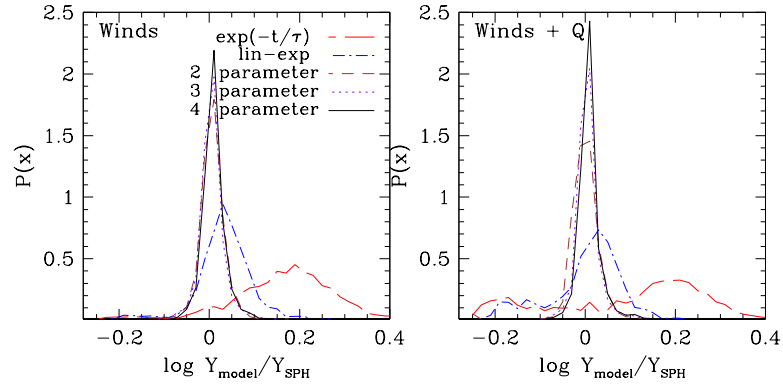


Figure 8. Distribution of differences between the r -band mass-to-light ratio predicted by the parametric models and that of the corresponding SPH galaxy, at $z = 0$. Each curve stands for a different parametric model, and the curves are normalised to unit integral.

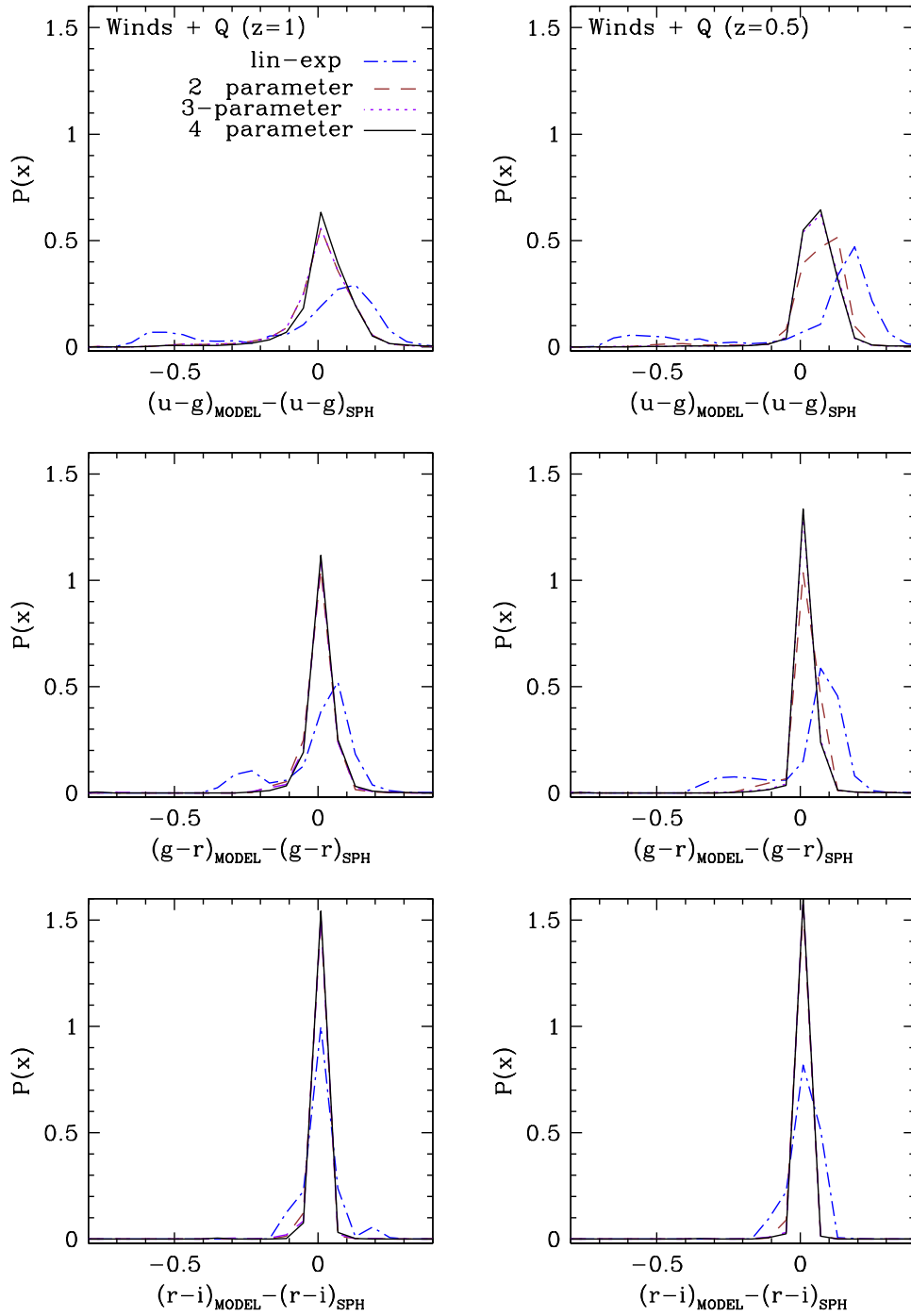


Figure 9. Distribution of differences between parametric model colour and SPH galaxy colour at $z = 1$ (left) and at $z = 0.5$ (right). Each curve stands for a different parametric model, and the curves are normalised to unit integral.

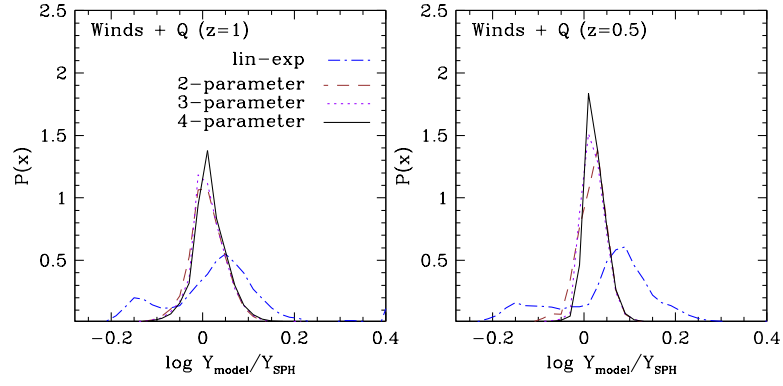


Figure 10. Distribution of differences between the r -band mass-to-light ratio predicted by the parametric models and that of the corresponding SPH galaxy at $z = 1$ (left) and $z = 0.5$ (right). Each curve stands for a different parametric model, and the curves are normalised to unit integral.

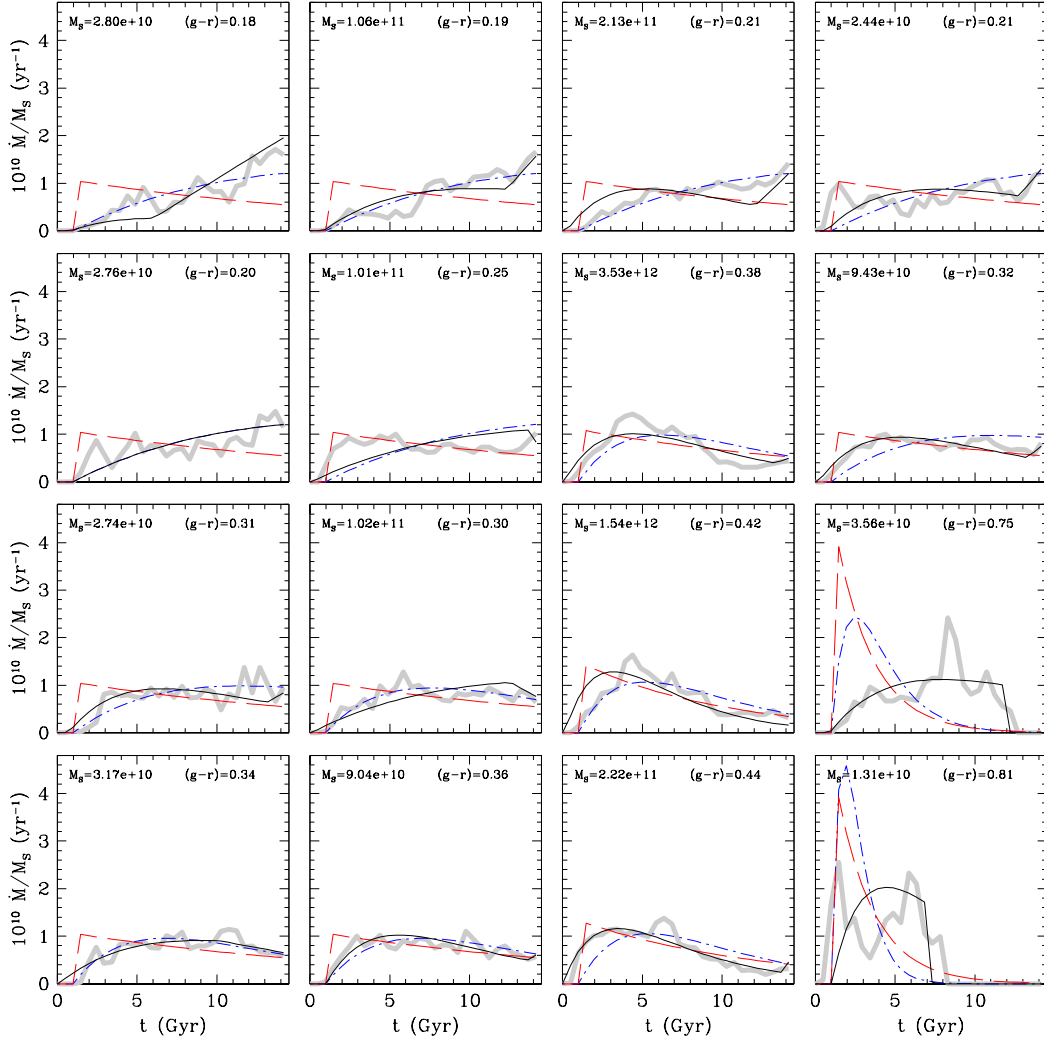


Figure 11. Galaxy SFR versus time in the winds simulation. Each panel shows an individual galaxy. We use the same set of galaxies as Figure 3 but with models fit to the $z = 0$ *ugriz* colours rather than SFH. The thick gray curve shows the SFR in the simulation, the black solid curve shows the best-fit 4-parameter model (see text), the blue dot-dashed curve shows the best-fit lin-exp model, and the red dashed curve shows the τ -model.

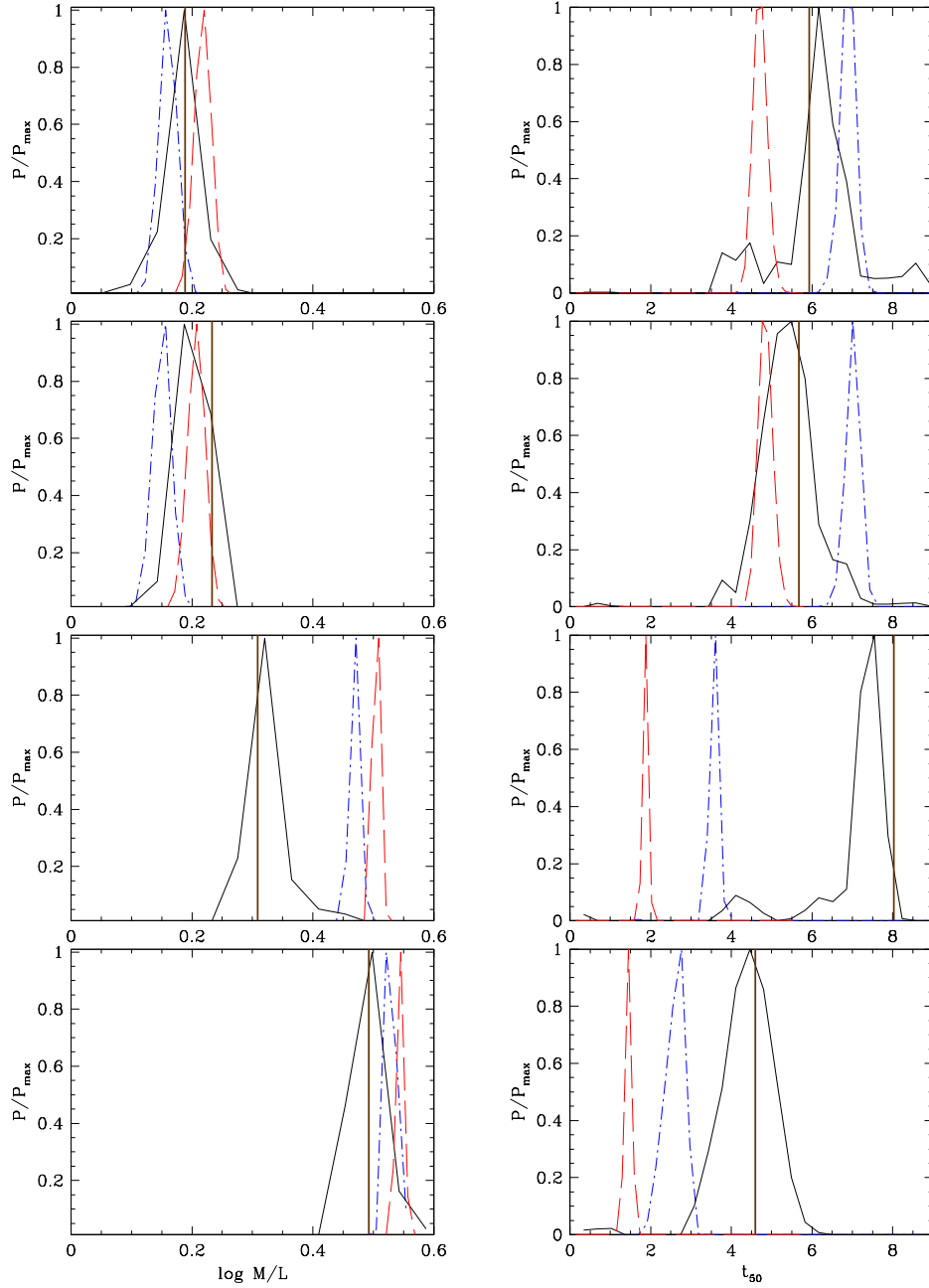


Figure 12. Posterior probability distribution of the r -band mass-to-light ratio (left) and t_{50} , the time at which 50% of the stars are formed (right), obtained by fitting parametric models to the $z = 0$ galaxy *ugriz* colours. Each row stands for a galaxy. Each curve stands for a particular parametric model - the 4-parameter model (solid black), the lin-exp model (blue dot-dashed), and the τ -model (red dashed). The grey solid line in each panel shows the “true” value of the mass-to-light ratio (left) and t_{50} (right) of the galaxy in the SPH simulation

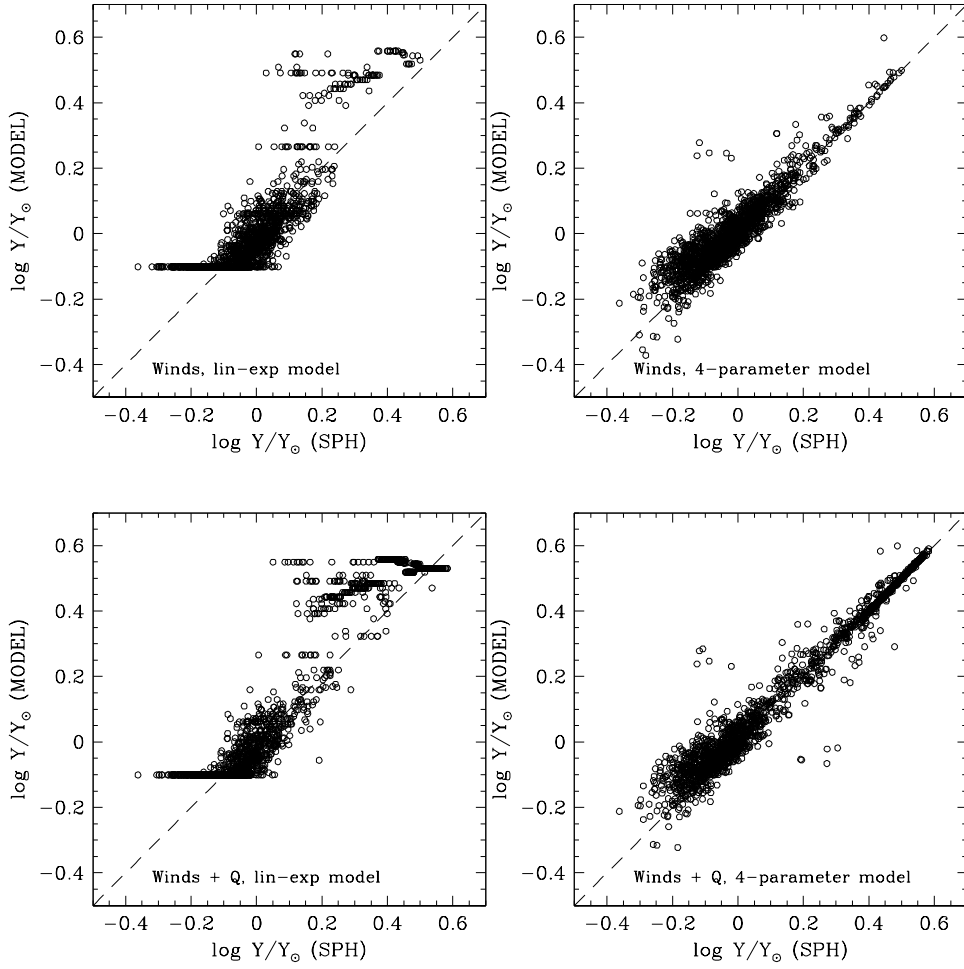


Figure 13. Mode of the posterior probability distribution of the mass-to-light ratio from parametric model SFH fits to $z = 0$ *ugriz* colours versus mass-to-light ratio of SPH galaxies. Each point is an individual galaxy. There are 1,828 galaxies plotted in the upper panels and 1,723 in the lower panels. The left panels show the lin-exp model and the right panels the 4-parameter model. The upper panels are fits to galaxies in the Winds population and the bottom panels to those in the Winds+Q population.

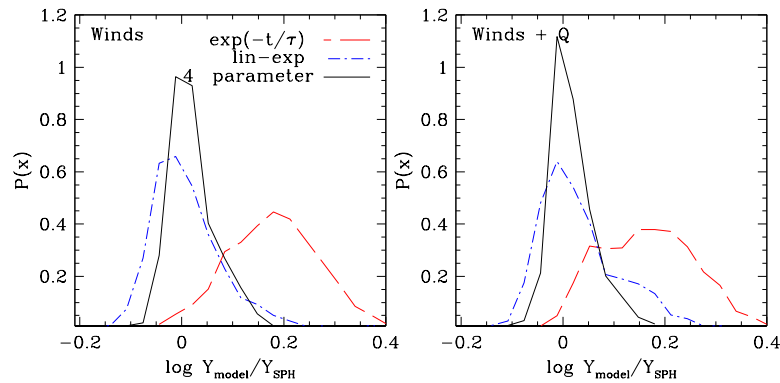


Figure 14. Distribution of differences between the r -band mass-to-light ratio predicted by the parametric model SFH fits to $z = 0$ *ugriz* colours and that of the corresponding SPH galaxy. Each curve stands for a different parametric model, and the curves are normalised to unit integral.

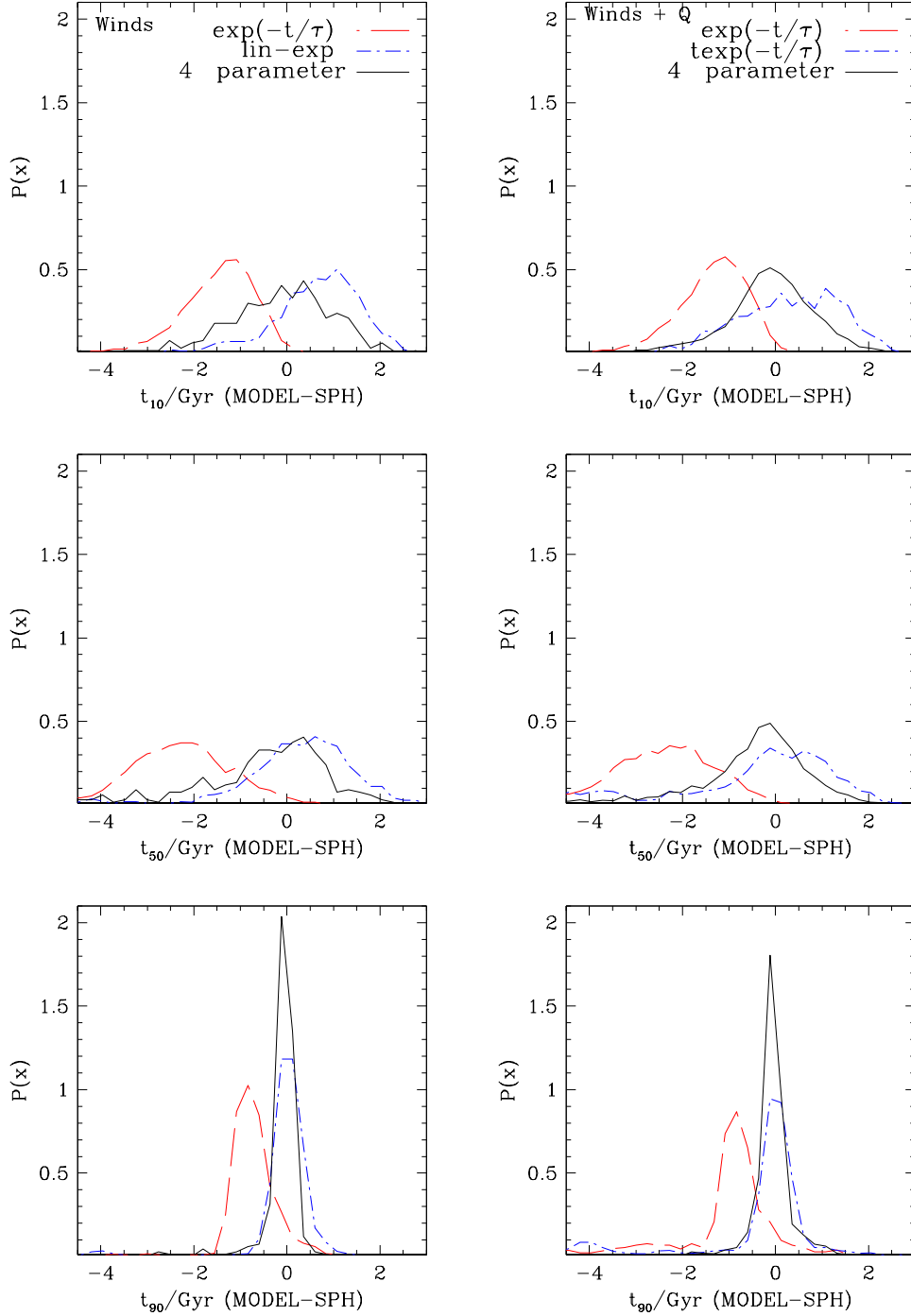


Figure 15. Distribution of differences between age of the galaxy stellar population predicted by the parametric model SFH fits to $z = 0$ *ugriz* colours and their age in the winds population (left) and the Winds + Q population (right). Each curve stands for a different parametric model and the curves are normalised so that the area under each curve integrates to unity. t_{10} , t_{50} and t_{90} stand for the time at which 10%, 50% and 90% of the stars were formed respectively.

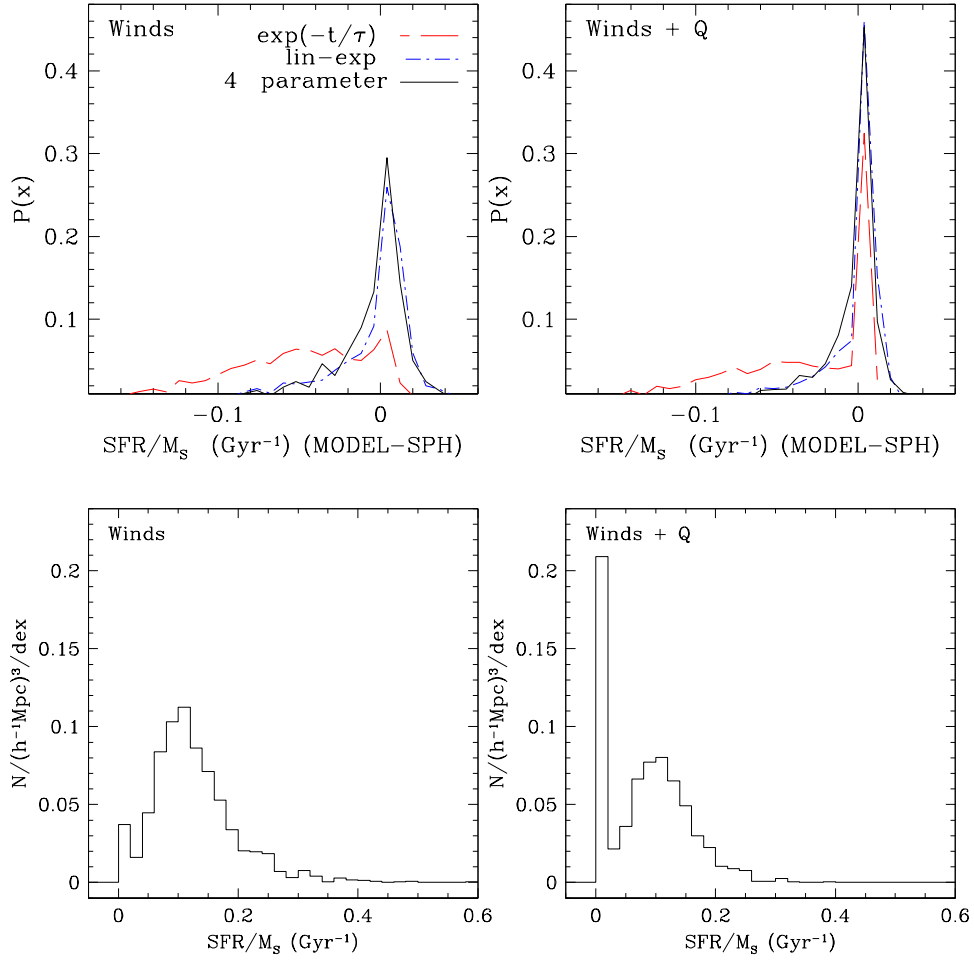


Figure 16. Distribution of differences between the specific star formation rate (sSFR) predicted by the parametric model SFH fits to $z = 0$ *ugriz* colours and the Winds population (top left) and the Winds + Q population (top right). Each curve stands for a different parametric model, and the curves are normalised to unit integral. Histograms in the two bottom panels show the distribution of sSFR in the two galaxy populations.

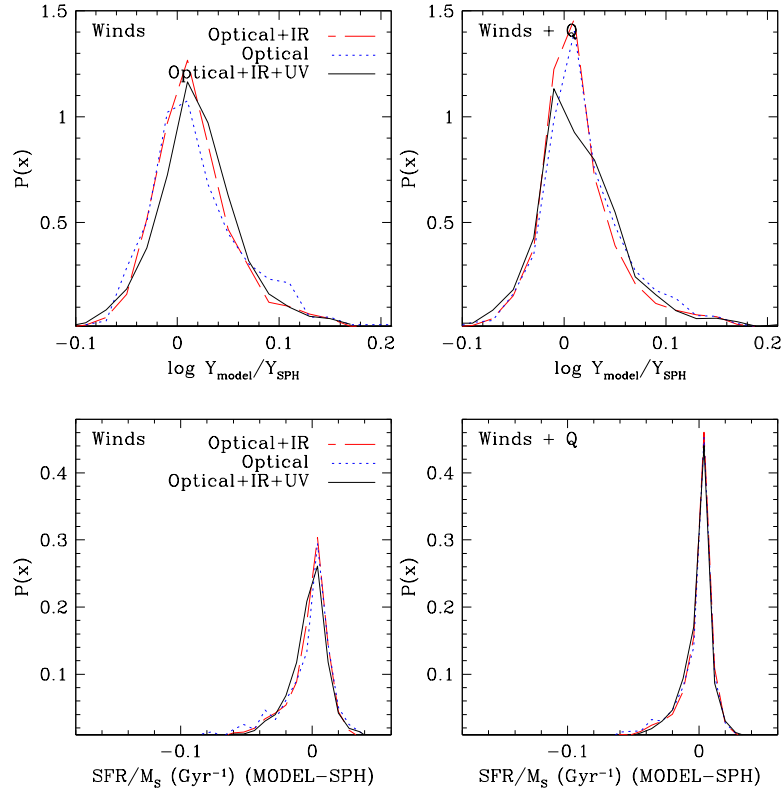


Figure 17. Impact of adding IR or IR+UV colours to optical colours when inferring the r -band mass-to-light ratio (top) or sSFR (bottom). Curves show the distribution of errors from fits of the 4-parameter model using optical colours only (dotted), optical+IR (dashed), or optical+IR+UV (solid).

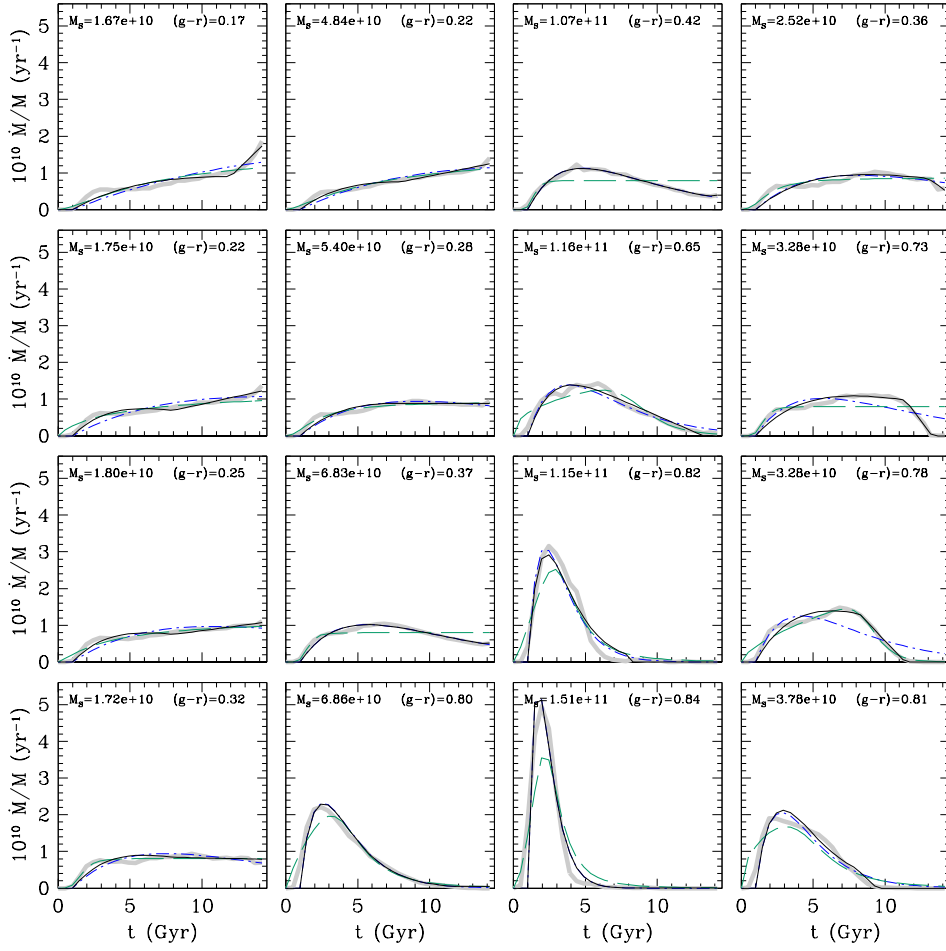


Figure 18. Same as Figure 5, but showing the Behroozi et al. (2013) SFH parametrization (long dashed green) fit to the average SFH of galaxies in bins of mass and colour in our Winds + Q population. For comparison, we also show the lin-exp model (blue dot dashed) and 4-parameter model (black solid) fits.

REFERENCES

- Agertz, O., et al. 2007, MNRAS, 380, 963
- Aubert, D., Pichon, C., & Colombi, S. 2004, MNRAS, 352, 376
- Barnes, J., & Hut, P. 1986, Nature, 324, 446
- Bell, E. F., & de Jong, R. S. 2001, ApJ, 550, 212
- Bell, E. F., McIntosh, D. H., Katz, N., & Weinberg, M. D. 2003, ApJS, 149, 289
- Berlind A. A., et al. 2003, ApJ, 593, 1
- Behroozi, P. S., Wechsler, R. H., & Conroy, C. 2013, ApJ, 770, 57
- Brinchmann, J., Charlot, S., White, S. D. M., Tremonti, C., Kauffmann, G., Heckman, T., & Brinkmann, J. 2004, MNRAS, 351, 1151
- Bruzual A., G. 1983, ApJ, 273, 105
- Conroy, C., Wechsler, R. H., & Kravtsov, A. V. 2006, ApJ, 647, 201
- Conroy, C., & Wechsler, R. H. 2009, ApJ, 696, 620
- Conroy, C., Gunn, J. E., & White, M. 2009, ApJ, 699, 486
- Conroy, C. 2013, ARA&A, 51, 393
- Coles, P., Lucchin, F., Matarrese, S., & Moscardini, L. 1998, MNRAS, 300, 183
- Colín, P., Klypin, A. A., Kravtsov, A. V., & Khokhlov, A. M. 1999, ApJ, 523, 32
- Davé, R., Katz, N., Oppenheimer, B. D., Kollmeier, J. A., & Weinberg, D. H. 2013, arXiv:1302.3631
- Davis M., Efstathiou G., Frenk C. S., & White S. D. M. 1985, ApJ, 292, 371
- Dekel, A., & Birnboim, Y. 2006, MNRAS, 368, 2
- Diemand, J., Moore, B., & Stadel, J. 2004, MNRAS, 352, 535
- Elbaz, D., et al. 2007, A&A, 468, 33
- Evrard, A. E., Summers, F. J., & Davis, M. 1994, ApJ, 422, 11
- Fall S.M., Efstathiou G. 1980, MNRAS, 193, 189.
- Förster Schreiber, N. M., et al. 2009, ApJ, 706, 1364
- Gabor, J. M., Davé, R., Oppenheimer, B. D., & Finlator, K. 2011, MNRAS, 417, 2676
- Gao, L., White, S. D. M., Jenkins, A., Stoehr, F., & Springel, V. 2004, MNRAS, 355, 819
- Gelb J.M., Bertschinger E. 1994, ApJ, 436, 467.
- Ghigna, S., Moore, B., Governato, F., Lake, G., Quinn, T., & Stadel, J. 1998, MNRAS, 300, 146
- Giavalisco, M., & Dickinson, M. 2001, ApJ, 550, 177
- Giavalisco, M., Ferguson, H. C., Koekemoer, A. M., et al. 2004, ApJL, 600, L93
- Guo, Q., White, S., Li, C., & Boylan-Kolchin, M. 2010, MNRAS, 404, 1111
- Haardt, F., & Madau, P. 2001, Clusters of Galaxies and the High Redshift Universe Observed in X-rays,
- Hernquist, L. 1987, ApJS, 64, 715
- Hockney, R. W., & Eastwood, J. W. 1981, Computer Simulation Using Particles, New York: McGraw-Hill, 1981,
- Katz, N., Hernquist, L., & Weinberg, D. H. 1992, ApJ, 399, L109
- Katz N., Weinberg D. H., Hernquist L. 1996, ApJS, 105, 19.
- Kauffmann, G., et al. 2003, MNRAS, 341, 33
- Kazantzidis, S., Mayer, L., Mastroiello, C., Diemand, J., Stadel, J., & Moore, B. 2004, ApJ, 608, 663
- Kereš, D., Katz, N., Weinberg, D. H., & Davé, R. 2005, MNRAS, 363, 2
- Kereš, D., Katz, N., Fardal, M., Davé, R., & Weinberg, D. H. 2009, MNRAS, 395, 160
- Kennicutt, R. C., Jr. 1998, ApJ, 498, 541
- Kitayama, T., & Suto, Y. 1996, ApJ, 469, 480
- Klypin, A., Kravtsov, A. V., Valenzuela, O., & Prada, F. 1999, ApJ, 522, 82
- Kravtsov, A. V., Berlind A. A., Wechsler R. H., Klypin A. A., Gottlöber S., Allgood B., Primack, J. R. 2004, ApJ, 609, 35
- Larson, D., et al. 2010, arXiv:1001.4635
- Lee, S.-K., Ferguson, H. C., Somerville, R. S., Wiklind, T., & Giavalisco, M. 2010, ApJ, 725, 1644
- Li, C., & White, S. D. M. 2009, MNRAS, 398, 2177
- Lee, S.-K., Idzi, R., Ferguson, H. C., Somerville, R. S., Wiklind, T., & Giavalisco, M. 2009, ApJS, 184, 100
- Mandelbaum, R., Seljak, U., Kauffmann, G., Hirata, C. M., & Brinkmann, J. 2006, MNRAS, 368, 715
- Mo, H. J., Mao, S., & White, S. D. M. 1999, MNRAS, 304, 175
- Moore, B., Quinn, T., Governato, F., Stadel, J., & Lake, G. 1999, MNRAS, 310, 1147
- Moster, B. P., Somerville, R. S., Maulbetsch, C., van den Bosch, F. C., Macciò, A. V., Naab, T., & Oser, L. 2010, ApJ, 710, 903
- Murali C., Katz N., Hernquist L., Weinberg D. H., Davé R. 2002, ApJ, 571, 1
- Nagai, D., & Kravtsov, A. V. 2005, ApJ, 618, 557
- Noeske, K. G., et al. 2007, ApJL, 660, L43
- Oppenheimer, B. D., & Davé, R. 2006, MNRAS, 373, 1265
- Oppenheimer, B. D., & Davé, R. 2008, MNRAS, 387, 577
- Oppenheimer, B. D., Davé, R., Kereš, D., Fardal, M., Katz, N., Kollmeier, J. A., & Weinberg, D. H. 2010, MNRAS, 406, 2325

- Oppenheimer, B. D., Davé, R., Katz, N., Kollmeier, J. A., & Weinberg, D. H. 2012, MNRAS, 420, 829
- Panther, B., Jimenez, R., Heavens, A. F., & Charlot, S. 2007, MNRAS, 378, 1550
- Papovich, C., Dickinson, M., & Ferguson, H. C. 2001, ApJ, 559, 620
- Pozzetti, L., et al. 2010, A&A, 523, A13
- Reid, B. A., et al. 2010, MNRAS, 404, 60
- Scannapieco, E., & Thacker, R. J. 2003, ApJL, 590, L69
- Schmidt, M. 1959, ApJ, 129, 243
- Scoville, N., Aussel, H., Brusa, M., et al. 2007, ApJS, 172, 1
- Shapley, A. E., Steidel, C. C., Erb, D. K., Reddy, N. A., Adelberger, K. L., Pettini, M., Barmby, P., & Huang, J. 2005, ApJ, 626, 698
- Sijacki, D., Vogelsberger, M., Kereš, D., Springel, V., & Hernquist, L. 2012, MNRAS, 424, 2999
- Simha, V., Weinberg, D. H., Davé, R., Gnedin, O. Y., Katz, N., & Kereš, D. 2009, MNRAS, 399, 650
- Simha, V., Weinberg, D. H., Davé, R., et al. 2012, MNRAS, 423, 3458
- Somerville, R. S., Primack, J. R., & Faber, S. M. 2001, MNRAS, 320, 504
- Springel V., Yoshida N., White S. D. M. 2001, New Astronomy, 6, 79
- Springel V., & Hernquist L. 2002, MNRAS, 333, 649
- Springel, V., & Hernquist, L. 2003, MNRAS, 339, 289
- Springel, V. 2005, MNRAS, 364, 1105
- Steidel, C. C., Giavalisco, M., Dickinson, M., & Adelberger, K. L. 1996, AJ, 112, 352
- Steidel, C. C., Adelberger, K. L., Giavalisco, M., Dickinson, M., & Pettini, M. 1999, ApJ, 519, 1
- Steidel, C. C., Adelberger, K. L., Shapley, A. E., Pettini, M., Dickinson, M., & Giavalisco, M. 2003, ApJ, 592, 728
- Taylor, E. N., Hopkins, A. M., Baldry, I. K., et al. 2011, MNRAS, 418, 1587
- Tojeiro, R., Wilkins, S., Heavens, A. F., Panther, B., & Jimenez, R. 2009, ApJS, 185, 1
- Trujillo-Gomez, S., Klypin, A., Primack, J., & Romanowsky, A. J. 2010, arXiv:1005.1289
- Vale, A., & Ostriker, J. P. 2004, MNRAS, 353, 189
- Vale, A., & Ostriker, J. P. 2006, MNRAS, 371, 1173
- Weinberg D.H., Colombi S., Davé R., Katz N. 2008, ApJ, 678, 6.
- Weinmann, S. M., van den Bosch, F. C., Yang, X., Mo, H. J., Croton, D. J., & Moore, B. 2006, MNRAS, 372, 1161
- Weinmann, S. M., Kauffmann, G., von der Linden, A., & De Lucia, G. 2010, MNRAS, 406, 2249
- Wetzel, A. R. 2011, MNRAS, 412, 49
- Wetzel, A. R., Tinker, J. L., Conroy, C., & van den Bosch, F. C. 2013, MNRAS, 432, 336
- White S.D.M., Rees M.J. 1978, MNRAS 183,341.
- York, D. G., Adelman, J., Anderson, J. E., Jr., et al. 2000, AJ, 120, 1579
- Zheng Z., et al. 2005, ApJ, 633, 791
- Zu, Y., Weinberg, D. H., Davé, R., Fardal, M., Katz, N., Keres, D., & Oppenheimer, B. D. 2010, arXiv:1005.4406